AD-A168 767 OPTICAL COMPUTING BASED ON THE HOPFIELD MODEL FOR NEURAL NETS(U) MOORE SCHOOL OF ELECTRICAL ENGINEERING PHILADELPHIA PA N H HART MAY 86 EO/MO-10 1/1

UNCLASSIFIED N00014-85-K-2036 F/G 6/4 NL

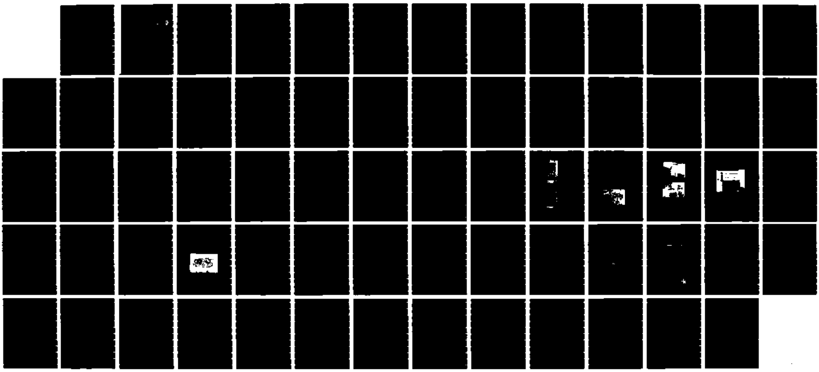

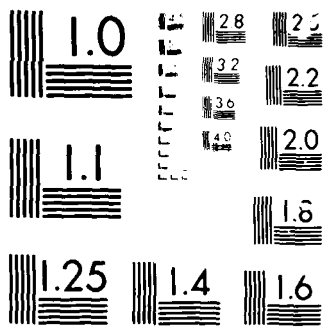

MICROCOP CHAR

University of Pennsylvania
The Moore School of Electrical Engineering
200 South 33rd Street
Philadelphia, PA 19104-6390

AD-A168 767

ANNUAL REPORT

OPTICAL COMPUTING BASED ON THE HOPFIELD MODEL FOR NEURAL NETS

Prepared by

N.H. Farhat

For

Naval Research Laboratory
4555 Overlook Ave., S.W.
Washington, D.C. 20375
Attn: Code 5709

Grant No. N00014-85-K-2036

May 1986

EO/MO Report No. 10

University of Pennsylvania
The Moore School of Electrical Engineering
200 South 33rd Street
Philadelphia, PA 19104-6390

ANNUAL REPORT

OPTICAL COMPUTING BASED ON THE HOPFIELD MODEL FOR NEURAL NETS

Prepared by

N.H. Farhat

For

Naval Research Laboratory
4555 Overlook Ave., S.W.
Washington, D.C. 20375
Attn: Code 5709

Grant No. N00014-85-K-2036

May 1986

EO/MO Report No. 10

TABLE OF CONTENTS

REPORT DISTRIBUTION LIST

	Copies
Naval Research Laboratory 4555 Overlook Ave., S.W. Washington, D.C. 20375 Attn: Code 5709	1
ONRR National Academy of Sciences 2100 Pennsylvania Ave., N.W. Washington, D.C. 20037-3202	1
Director Naval Research Laboratory 4555 Overlook Ave., S.W. Washington, D.C. 20375 Attn: Code 2627	6
Defense Technical Information Center Bldg. 5, Cameron Station Alexandria, VA 22314	12
Program Management Office 1400 Wilson Blvd. Arlington, VA 22209-2308 Attn: Dr. John Neff	1

ABSTRACT

Neural net models and their analogs present a new approach to signal processing that is collective, robust, and fault tolerant. The collective nature of processing means also high throughput where bandwidth or speed of the processing elements i.e., temporal degrees of freedom are traded by spatial degrees of freedom via massive interconnectivity of the elements (neurons) in the network. As a result neural nets can solve computationally extensive problems like those encountered for example in optimization, nearest neighbor search, inverse scattering in a matter of a few time-constants of the processing elements. In biological systems (the brain in particular) this is of the order of a tens of milliseconds since neurons operate with ionic conduction. Artificial semiconductor based neurons operate with electronic conduction and hence can be made considerably faster with time constants approaching nano-seconds. Collective processing such artificial nets can therefore be extremely fast. The remarkable ability of neural nets in handling sketchy (erroneous or incomplete) information and their fault tolerance (graceful degradation in performance with element failure) make them particularly attractive in pattern recognition, robotics, and autonomous system intended to operate virtually unattended for long time periods.

In this report we describe progress during the past year in our study of optical computing based on the Hopfield model of neural networks and other similar models. Optical implementations are of interest because they furnish the parallelism and massive interconnectivity required in implementing neural net models. At the same time neural net models provide

optics with robustness, fault tolerance, and the power of nonlinear feedback.

To gain insight in the ultimate utility of analog neural net processing as opposed to conventional analog or digital processing we have also addressed the question of applications by choosing to study (a) the utility of neural net processing in the important area of radar target recognition employing realistic data generated in our Experimental Microwave Imaging Facility and (b) the optimization of radiation patterns of phased array antennas.

The work described encompasses a general survey of assessment of the field, study of methods for further simplification of optical implementations of content addressable associative memory without sacrifice in performance, study of optical analogs of 2-D neural nets with the aim of implementing denser networks suitable for processing 2-D image classifiers or feature spaces, study of automated radar target recognition based on models of neural nets and the use of sinogram classifiers, and the optimization and synthesis of phase array antennas.

The results obtained appear to attest to the viability of neural net models and their optical analogs as a new and powerful approach to signal processing and provide impetus for their further study.

1. INTRODUCTION

Interest in neural network models (see for example, [1]-[9]) and their opto-electronic analogs stems from well recognized capabilities of the brain and the fit between what optics can do and what even simplified models of neural nets can offer toward the development of new approaches to collective signal processing. We know that the brain is not as good in arithmetic operations as a digital computer but when it comes to operations such as association, categorization, generalization, classifiction, feature extraction, recognition, and optimization it outperforms even the most powerful of todays computers. The brain's amazing capabilities in analyzing sensory data and in controlling motor function, let alone complex thought and intelligent reasoning, makes it an intriguing model for smart sensing and automated recognition systems and for robotic and automatic control systems with unescapable ramification for pattern recognition, artificial intelligence and autonomeous systems. An interesting aspect of its ability in processing sensory data is the ease with which it solves computationally complex problems associated for example with vision that are basically inverse problems [10]. These are computationally vexing because of their ill-posedness [11]. The brain's associative memory capabilities where nearest neighbor searches are performed successfully even when the information it is presented with is sketchy are evidence of its remarkable robustness where high levels of missing or erroneous data in the input can be tolerated. The ability of the brain to supplement missing information has exciting implications for super-resolution and other similar problems of signal recovery from incomplete and noisy data [11],[12]. The capabilities of the brain in rapid solution of optimization problems [13] are also well appreciated. Add to the above that the brain is amazingly fault tolerant as

its (cells or neurons), unlike cells in other parts of the body, are not renewable. Yet, despite loss of a non-negligible number of cells by the time one of us reaches the age of 50 we continue to function normally. We know something about how the brain processes information. We know that it does that in parallel or more precisely collectively by means of massively interconnected networks of neurons. There are anywhere between 10^{10}- 10^{11} neurons in the brain, each making about 10^3- 10^4 synaptic interconnections with neighboring neurons for a total of 10^{13} to 10^{15} interconnections. Even when we assume the neuron to take only two states: firing or not firing i.e., binary neuron, the total number of degrees of freedom of the the brain is truly astronomical reaching $2^{10^{15}}$. Each neuron independently evaluates its state and decides to change it or not depending on whether the sum of its synaptic (exitatory and inhibitory) inputs exceeds a given threshold or not performing thus a highly nonlinear (logic) operation.

Massive connectivity and parallelism are the two main attributes of optics. Optics can therefore play an important role in the implementation of models of neural nets for computing and signal processing. Besides developments in programmable nonvolatile spatial light modulators [14], optical light amplifiers [15], and optical bistability devices [16] promise to play a useful role in the implementations of programmable connectivity matrices, and optical decision making elements leading ultimately to powerful neural net type processors.

The above observations have served as motivation for several workers [17]-[31] to investigate the feasibility and capabilities of optical implementations of neural nets. Optical implementations of 1-D and 2-D distributions of neurons (neural nets) have been considered and/or studied

and evaluated in coherent and incoherent light. The performance of such networks is found to conform to theoretical prediction of storage capacity (number of entities that can be reliably stored) [32]-[34], and exhibits robustness and fault tolerance. In an optical implementation of an associative memory of N=32 neurons, with three stored entities errors of up to 30% in the input stimulus was tolerated during complete and correct recall of the nearest neighbor stored entity. Furthermore, accidental failure of about 10% of the neurons hardly caused noticable degradation in performance. Some of the above studies have been aimed at finding means of simplifying optical implementation of large neural nets, increasing the storage capacity, and finding ways for their interconnections as modules into more complex systems to perform higher order hierarchical processing.

It is worth noting that operations such as associative recall and nearest neighbor search performed in the above systems can be carried out by more conventional means without resort to neural net processing. What does the neural net approach then offer that conventional signal processing and computing methods do not?. The answer to this question may be found in the following observations: (a) Neural nets and their models provide us with a new way of viewing signal processing and computing problems that may lead to solutions and applications not thought of otherwise in a manner very much reminiscent to what happened with the advent of holography several decades ago. (b) The brain and its neural organization are the results of a prolonged evolutionary process in which only those permutations that enhanced the survivability, and by implication the function, of the organism have been retained and all other permutations have been discarded through "survival of the fittest" process. The result is a biological "computer" that has, as pointed out earlier, no equal at present among artificial

systems when it comes to tasks of recognition, classification, categorization, generalization, recognition, and optimization. It is not surprising therefore to see the current interest in brain mechanisms in the artificial intelligence, cognitive science, and pattern recognition communities. Even early researchers in computer science were concerned with brain-related attributes of computing systems [35]. A serial approach to computing was however adopted and pursued because of better understanding, easier mathematical modeling, and possibly because a collective or parallel approach to computation would have been technologically and economically not feasible at the time. There is much therefore that we can afford to learn from the brain and its neural nets that can prove to be useful in artificial man made systems. The general idea here is not to attempt to build systems that fully emulate the brain in all its functions, as this would be unrealistic, but to gain insights in its operation and mechanisms, as to allow us to be able to glean information about these attributes and functions that would be worth incorporating in man made systems. Optical analogs of neural nets can be a useful tool in gaining such insights and as a way of ultimately simulting neural nets consisting of thousands to millions of elements. (c) Information processing in the brain can be characterized as collective, adaptive, highly nonlinear, and relying heavily on feedback. We know that all these are attributes of powerful signal processing algorithms. What is amazing is that these capabilities are achieved in networks that appear to be homogeneous in their general structure i.e., only a few different types of neurons (cells) are involved and the process followed by most neurons is macroscopically similar in the sense that each neuron receives inputs from other neighboring neuron and decides to change its state or not depending on the nature of the inputs and

the synaptic weights they make with the neuron where memory is stored. In other words the brain exhibits a fractal (self-similar) feature in its organization. It is now recognized that the same basic structure of highly interconnected neurons can be involved in the formation of signal-adaptive self-organized networks for unsupervised learning and feature extraction from sensory data [4],[36], in the formation of associative memory modules tuned to respond to specific features of the sensory data, [37]-[41] and for recognition and perception "circuits" of the brain. This is a tremendous flexibility that is achieved with little apparent specific design unlike conventional circuit design where function specific components and parts are connected in accordance to specific rules to perform required signal processing tasks. As evidence of this flexibility it is worth noting in this regard that in associative memory based on neural net models the function of memory and signal processing involved in recall are totally intermingled. (d) The fractal nature of neural nets, their robustnewss and fault tolerance can be immensely useful for modern VLSI technology. Continuing advances in microfabrication, and optical technologies promise to make it possible to fabricate large numbers of massively interconnected decision making switching elements with low power consumption. Neural net models and architectures can provide such structures (possibly in the form of opto-electronic chips) with the robustness and the fault-tolerance badly needed in VLSI to alleviate the central problem of yield. Imperfect chips may no longer be regarded as rejects but can find use in artificial neural net processors or computers. (e) Architectures and Optical implementations of 2-D neural net arrangements can provide content addressable associative memory modules that are suited for use with 2-D pictorial data. In practice such pictorial data would be in the form of distortionless descriptors, (scale,

rotation, and size invariant classifiers or feature spaces) derived from sensory array data generated for example by electromagnetic or acoustic (including seismic and sonar) receiver arrays. Associative memory modules can tell us then rapidly, in a matter of a few time constants of the neuron-like elements used, which member of an ensemble of input descriptors is recognized by the memory even when the descriptor information it is presented with happens to be incomplete or sketchy. Recognition of an input is manifested by the neural net converging and settling into one of its nominal states corresponding to that stored entity which most resembles the input. It is clear that this operation by itself may not be useful unless some means for identifying or recognizing the outcome of the nearest neighbor search is incorporated. This suggests, in the absence of such "recognizer", that auto-associative memories may be useful as building blocks of more complex processors in which higher order hierarchical processing takes place, in a manner not yet fully understood. Such processing would have the aim of first reducing the information content of the signals flowing concurrently through such a network of associative CAMs and then fusing their outcomes into a single meaningful concept or perception. In biological systems, such perception is thought to be associated with a prescribed trace of neural activity or spatio-temporal firing pattern in the cortex. Associative memory modules by themselves become more meaningful when used in a hetero-associative mode where the learning set of descriptors or classifiers is not stored by auto-association but by hetero-association with reference entities that are more easy to recognize i.e., reference entities that are compatible with the "recognizer" such as word labels or pictorial representations in the case of a human observer or coded analog or digital outputs suitable for activating motor

functions in robotic and artificial intelligence systems. Hetero-associative storage and recall of partial information can play an important role in smart sensing and automated recognition systems as was recently demonstrated with an example of identifying different types of aircraft from partial information about their sinogram classifiers [42] and individual faces from edge enhanced versions as classifiers [43].

2. RESEARCH ACCOMPLISHMENTS

Neural net models and their optical analogs provide a new approach to signal processing. The aim of our research activity during the period of this report was therefore to study and assess the capability of neural net processing in actual challenging applications where they are expected to be most useful such as automated recognition. To this aim we have also paid attention to the question of optical implementation of large neural nets of the type we expect is needed in smart sensing and automated recognition applications. Therefore our research efforts during the preceeding period have focused specifically upon the following tasks:

(a) Study of methods for simplifying optical implementations of neural net models without sacrificing performance. To this purpose a systematic numerical study of optical embodiments that employ different types of synaptic or connectivity masks (e.g., multivalued, ternary, unipolar binary) and a variety of thresholding methods (e.g., zero thresholding, adaptive thresholding where the threshold is proportional to the energy of the initiating and iterated input, adaptive thresholding and relaxation where the neuron is influenced by its previous state - self inhibition) were studied and their performance compared. The

results of this study are detailed in Appendix I of this report. They show that the adaptive thresholding and relaxation scheme can be used with a unipolar binary (u.b.) mask without suffering any degradation in performance as compared to the ideal case when zero thresholding and a multivalued mask are employed. The ability to use a u.b. connectivity mask enables their realization in black-and-white optical transparencies and opens the way for the use of nonvolatile spatial light modulators for computer driven programmable connectivity matrices.

(b) Numerical simulation and experimental study of optical analogs of 2-D distributions of neural nets (2-D neural nets) based on a novel scheme for partitioning the resulting 4-D connectivity matrix into a 2-D array of 2-D matrices was undertaken. Architectures based on this matrix partitioning scheme were studied numerically and found to work efficiently. The primary motive for our interest in 2-D neural nets is their compatability with 2-D feature space data and their potential for realizing dense neural nets of $\sim(10^3-10^4)$ elements. The results of this task are detailed in Appendix II of this report. There the application of a 2-D neural net of 32x32 elements in an automated recognition situation namely, recognition of scale models of three aero-space targets employing sinogram representations or feature spaces of these targets produced employing a unique microwave measurement facility is described in some detail. Super-resolved recognition employing partial information ($\gtrsim 20\%$) of the sinogram data of the three test objects and making use of a hetero-associative memory whose output at the completion of a successful

search is a label of the corresponding recognized object is demonstrated. The use of realistic data in this work is important as it illustrates, together with the ability to recognize the input when it is partial and sketchy, the unusual robustness of neural net models and their analogs. The results presented in Appendix II exhibit also a certain degree of generalization when the memory output is a composite of the entities it was taught. This occurs only if the amount of information it is presented with is meager (e.g., 10% or less of a full sinogram pattern). These results seem to underline the uniqueness of the neural net approach to signal processing in that complex functions are realized in self similar nets of interconnected neurons as opposed to conventional signal processing schemes and architectures based on a highly organized modular approach.

(c) Initiation of construction of a 2-D neural net of 5x5 element to be used as a test bed leading to eventual construction of 16x16 and then 32x32 neural nets. All of these embodiment utilize a lenslet array to multiplex the initiating external input and the iterated input onto the partitions of the 4-D connectivity matrix $T_{ijk\ell}$ and nonlinear electronic feedback loops from an output monitoring photodetector array paired with an LED array at the input.

(d) Collective processing is recognized to be an effective tool in the solution of combinatorial problems. Both neural net based algorithms and similar simulated annealing algorithms are applicable. We have initiated a study of this important area by considering the novel problem of synthesizing an optimal radiation

pattern of a phased array antenna by simulated annealing. The results of this study are detailed in Appendix III. The results show that simulated annealing can be a useful tool in phased array synthesis. The attractiveness and effctiveness of the method can be considerably enhanced if the computation times required are reduced. Hybri (opto-digital or opto-electronic) schemes can play a role here. Their applicability is being investigated.

3. CONCLUDING REMARKS

At this stage of their early development one can only venture to say that neural net models offer a new and intellectually stimulating approach to computing and information processing. The approach "dove-tails" very well with the capabilities of optics and compliments them. While optics naturally provides the parallelism and massive interconnectivity needed in the implementation of neural nets and their models, these on their part provide the robustness, fault tolerance, and the power of nonlinear processing and feedback that are generally lacking in optical processing. The combination results in systems that can no longer be characterized by the usual measures of convolution and impulse response (variant or invariant) because superposition no longer applies but may have to be characterized instead by stable states or modes in the N-dimensional phase-space of an N-neuron network. Optical analogs of even highly simplified models of neural nets exhibit a high degree of robustness and fault-tolerance, and can be implemented as content addressable associative memories for use in computers and in smart sensing and automated recognition systems, or as networks for rapid collective solution of computationally complex tasks encountered in optimization, vision, and inverse problems.

They may also provide a tool for the study of nonlinear dynamics, chaos, and even prove to be useful in clinical studies of mental disorder.

4. OTHER ACTIVITIES

During the period of this report papers were presented at the following conferences and meetings.

1. N.H. Farhat and D. Psaltis, "Architectures for Optical Implementation of 2-D Content Addressable Memories", Digest OSA Annual Meeting, Wash. D.C., p. 58, 1985.

2. K.S. Lee and N.H. Farhat, "Content Addressable Memory with Smooth Transition and Adaptive Thresholding", Digest OSA Annual Meeting, Wash. D.C., p. 48, 1985.

3. N. Farhat, K.S. Lee and Lie-Szu Chang, "High-Speed Fourier Camera", Digest OSA Annual Meeting, Wash. D.C., p. --, 1985.

4. D. Psaltis, E.G. Paek, J. Hong and N. Farhat, "Acousto-Optic Implementation of Neural Network Models", *Digest OSA Annual* Meeting, Wash. D.C., p. 58, 1985.

5. N. Farhat, "Optical Implementations of Associative Memory", DARPA/DSO-AFOSR/NC Optical Processing Annual Review, BDM International, Inc., McLean, Va., Nov. 1985.

6. N. Farhat, "Microwave Diversity Imaging and Automated Target Recognition", Reconnaissance, Surveillance and Target Acquisition (RSTA) SYMPOSIUM, Harry Diamond Laboratories, Adelphi, Maryland, Jan. 1986. (Invited)

7. N. Farhat and S. Miyahara, "Super-resolution and Signal Recovery Using Models of Neural Networks", Technical Digest, Spring 86 OSA Topical Meeting on Signal Recovery and Synthesis II, pp. 120-123, 1986.

8. N. Farhat, S. Miyahara and K.S. Lee, "Optical Implementations of 2-D Neural Nets and their Application in Recognition of Radar Targets", Presented at the Neural Networks for Computing Conference, Snowbird, Utah, 1986.

5. REFERENCES

1. Widrow, B. and M.E. Hoff, "Adaptive Switching Circuits", WESCON Convention Record, Part IV, pp. 96-104, 1960. Also in Self-Organizing Systems, M.C. Yovitz, et. al. (Eds.) Spartan 1962.

2. Nakano, K., "Association-A Model of Associative Memory", IEEE Trans. on Systems Man & Cybernetics., Vol. SMC-2, pp. 380-388, 1972.

3. Kohonen, T., "Correlation Matrix Memories", IEEE Trans. on Computers, Vol. C-21, pp. 353-359, (1972).

4. Kohonen, T., Associative Memory, Springer Verlag, Heidelberg (1978). Also "Self-Organization and Associative Memory", Springer Verlag, (1984).

5. Willshow, D.J., "A Simple Network Capable of Inductive Generalization", Proc. Roy. Soc. London, Vol. 182, pp. 233-247, 1972.

6. Anderson, J.A., et. al., "Distinctive Features, Categorical Perception, and Probability Learning: Some Applictions of a Neural Model", Physilogical Review, Vol. 34, pp. 413-451, 1977.

7. Hopfield, J.J., "Neural Networks and Physical Systems with Emergent Collective Computational Abilities", Proc. Natl. Acad. Sci., USA, Vol. 79, pp. 2554-2558, 1982. Also, "Neurons with Graded Response Have Collective Computational Properties Like Those of Two-State Neurons", Proc. Natl. Acad. Sci., USA, Vol. 81, 1984.

8. Grossberg, S., Studies of Mind and Brain, R. Reidel Pub. Co., Boston, 1982.

9. Sanderson, A.C., and Y.Y. Zeevi, (Eds.), Special Issue on Neural and Sensory Information Processing, IEEE Trans. on Syst. Man and Cybernetics, Vol. SMC-13, 1983.

10. Tikhonov, A.N. and V.Y. Arsenin, "Solutions of Ill-Posed Problems", Winston and Sons, Washington, D.C. 1977.

11. Poggio, T. and C. Koch, "Ill-Posed Problems in Early Vision: From Computational Theory to Analog Networks", Proc. Roy. Soc. London, Vol. B226, pp. 303-323, 1985.

12. Farhat, N. and S. Miyahara, "Super-resolution and Signal Recovery Using Models of Neural Networks", Technical Digest, Spring 86 OSA Topical Meeting on Signal Recovery and Synthesis II, Honolulu, Hawaii, pp. 120-123, 1986.

13. Hopfield, J.J. and D.W. Tank, "Neural Computations of Decisions in Optimization Problems", Biol. Cybernetics, Vol. 52, pp. 141-152, 1985.

14. Ross, W., D. Psaltis, and R. Anderson, "Two-Dimensional Magneto-Optic Spatial Light Modulator for Signal Processing", Optical Engineering, Vol. 22, pp. 485-490, 1983.

15. Porada, Z., "Thin Film Light Amplifier with Optical Feedback", Thin Solid Films, Electronics and Optics, Vol. 109, pp. 213-216, 1983.

16. Gibbs, H.M., and N. Peyghambrian, "Nonlinear Optical Mechanisms and Devices for Optical Computing", Technical Digest, OSA Topical Meeting on Optical Computing, Incline Village, Nev. pp. MC1-1 o MC1-3.

17. Psaltis, D. and N. Farhat, "A New Approach to Optical Information Processing Based on the Hopfield Model", Digest of the 13-th Congress of Intern. Commiss. on Optics, ICO-13, Saporro, Japan, 1984. Also, "Optical Information Processing Based on Associative-Memory Model of Neural Nets with Thresholding and Feedback", Opt. Lett., Vol. 10, pp. 98-100, 1985.

18. Farhat, N.H., et. al., "Optical Implementation of the Hopfield Model", App. Optics, Vol. 24, pp. 1469-1475, 1985.

19. Farhat, N.H., and D. Psaltis, "Architectures for Optical Implementation of 2-D Content Addressable Memories", Digest OSA Annual Meeting, Wash., D.C., p. 58, 1985.

20. Lee, K.S. and N.H. Farhat, "Content Addressable Memory with Smooth Transition and Adaptive Thresholding", Digest OSA Annual Meeting, Wash., D.C., p. 48, 1985.

21. Psaltis, D., et. al., "Acousto-Optic Implementation of Neural Network Models", Digest OSA Annual Meeting, Wash. D.C., p. 58, 1985.

22. Condon, D.J., et. al., "Optical Window Addressable Memory", OSA Topical Meeting on Optical Computing, Incline Village, Nov. 1985, (Post deadline paper).

23. Fisher, A.D., C.L. Giles, and J.N. Lee, "Associative Processor Architectures for Optical Computing", J. Opt. Soc. Am., A, Vol. 1, p. 1337, 1984. Also, "An Adaptive, Associative Optical Computing Element", Technical Digest, OSA Topical Meeting on Optical Computing, Incline Village, Nev., pp. WB4-1 to WB4-4, 1985.

24. Fisher, A.D., and C.L. Giles, "Optical Adaptive Associative Computer Architectures", Proc. of the IEEE COPCOM Spring Meeting, IEEE Computer Society, IEEE Cat. No. CH2135-2/85/0000/0342, pp. 342-334, 1985.

25. Fisher, A.D., et. al., "Implementation of Adaptive Associative Optical Computing Elements", SPIE, Vol. 625, Bellingham, WA., 1986.

26. Sofer, B., et. al., "Associative Holographic Memory with Feedback, Using Phase-Conjugate Mirrors", Opt. Lett., Vol. 11, pp. 118-120, 1986.

27. Anderson, D.Z., "Coherent Optical Eigenstate Memory", Opt. Lett. Vol. 11, pp. 56-58, 1986.

28. Yariv, A. and S.K. Kwong, "Associative Memories Based on Message-Bearing Optical Modes in Phase-Conjugate Resonator", Opt. Lett., Vol. 11, pp. 186-183, 1986.

29. Psaltis, D. et. al., "Shift Invariance in Optical Associative Memories", SPIE, Vol. 625, Bellinghm, WA., 1986.

30. Cohen, M., "Distributed Computation in Neural Networks and Their Optical Analogs", OSA Topical Meeting on Optical Computing, Incline Village, Nev., 1985. (Post deadline paper).

31. Mirsalehi, M.M. and T.K. Gaylord, "Multi-Level Coded Residue-Based Content-Addressable-Memory Optical Computing", Technical Digest, OSA Topical Meeting on Optical Computing, Incline Village, Nev., pp. WB4-1 to WB1-4, (1985).

32. Abu-Mustafa, Y.S. and J.M. St. Jacques, "Information Capacity of the Hopfield Model", IEEE Trans. on Inf. Theo., Vol. IT-31, pp. 461-464, 1985.

33. McElice, R.J., et. al., "Capacity of the Hopfield Associative Memory", Caltech Report, 1986.

34. Venkatesh, S. and D. Psaltis, "Information Storage and Retrieval in Two Associative Nets", Submitted to IEEE Trans. on Info. Theo.

35. Von Neuman, J., Probabilistic Logics and Synthesis of Reliable Organism From Unreliable Components in Automata Studies, C.E. Shannon and J. McCarthy (Eds.), Princeton Univ. Press, Princeton, N.J., pp. 48-98, 1956.

36. Fukushima, K., "Neocognition:A Self-Organizing Neural Network Model for a Mechanism of Pattern Recognition Unaffected by Shift in Position", Biol., Cybern., Vol. 36, pp. 193-202, 1980.

37. Hubble, D.H., "The Visual Cortex of the Brain",Scientific American, Vol. 209, pp. 54-63, 1963.

38. Hubble, D.H., and T.W. Weisel, "Functional Architecture of Macaque Monkey Visual Cortex", Proc. Roy. Soc. Lond. B., Vol. 198, pp. 1-59 1977.

39. Tootel, R.B., et. al., "Spatial Frequency Columns in Primary Visual Cortex", Science, Vol. 214, pp. 813-815, 1981.

40. Orban, G.A., Neuronal Operations in the Visual Cortex, Springer-Verlag, New York, see for example, sections 7.3.4 and 15.1.3., 1984.

41. Jones, J.P., and L.A. Palmer, "Simple Receptive Fields of Cat Striate Cortex: A Comparison with Gabor Functions in Two Dimensions of Space and Two Dimensions of Spatial Frequency", University of Pennsylvania - private communication, 1985.

42. Farhat, N. et. al., Optical Implementation of 2-D Neural Nets and Their Application in Recognition of Radar Target", Presented at the Neural Networks for Computing Conference, Snowbird, Utah, 1986.

43. Psaltis, D., et. al., "Nonlinear Discriminant Functions and Associative Memories", Presented at the Neural Networks for Computing Conference, Snowbird, Utah, 1986.

6. APPENDICES

APPENDIX I

CONTENT ADDRESSABLE MEMORY WITH SMOOTH TRANSITION AND ADAPTIVE THRESHOLDING

Kang S. Lee and Nabil H. Farhat
University of Pennsylvania
The Electro-Optics and Microwave-Optics Laboratory
200 S. 33rd street
Philadelphia, PA 19104

ABSTRACT : The use of unipolar binary masks and adaptive smooth thresholding in optical implementations of neural nets appears to combine the better performance of multi-level masks and ease of realization.

ABSTRACT : The use of unipolar binary masks and adaptive smooth thresholding in optical implementations of neural nets appears to combine the better performance of multilevel masks and ease of realization.

1. INTRODUCTION

Optical implementaion of the Hopfield model of neural nets may offer advantages over micro-electronic implementations because of the inherent parallelism of optical processing and the relative ease with which massive interconnectivity can be realized. As the number of stored patterns or entities increases, the elements of the memory or synaptic matrix will assume values extending over a wider range. This means a wider range of grey levels in the optical mask is required. For ease of optical implementaion, quantization into a bipolar binary (BB) mask or even into a unipolar binary (UB) mask would be desirable. In this paper we examine the use of UB masks with adaptive thresholding and a smooth or graded "neuron" response in the feed-back loop. For the UB mask a non-zero thresholding value must be adopted. Since the given information in the input vectors is contained in bits of zeros and ones, one half of the input vector energy suggests itself as a possible sharp thresholding level. As each iteration proceeds, the weighted projection of the current iterate is applied to an adaptive sharp thresholding unit. The result (negative, zero, or positive values depending on whether the projection is smaller, equal, or greater than one half the input energy) is multiplied by relaxation parameter, of value less than one, then combined with the previous iterate and is finally limited to [0,1]. In this way we realize a smooth transition of states for the neural net. The smooth

transition method is also related to the relaxation techniques used in solving systems of linear equations. Results of digital simulation are presented for a 32 neuron system. These are shown, as far as storage capacity and error correction are concerned, to compare favorably with performance of a multi-valued mask where merely sharp thresholding is used. Preliminary experimental results obtained with a modified version of a previously reported 32 neuron optical network are also given.

2. OPTICAL IMPLEMENTAION OF CONTENT ADDRESSABLE MEMORY (CAM) USING A BIPOLAR BINARY MASK

Several schemes for optical implementaion of a CAM based on the Hopfield model [1] and other similar models [2],[3] have been described earlier [4]-[7]. In one of the implementa- ions an array of light emitting diodes (LEDs) is used to represent the logic elements or neurons of the network. Their state (on or off) can represent unipolar binary vectors that are stored in the memory matrix T_{ij} employing the usual storage recipe [1]. Global inter-connection of the elements is realized as shown in Fig. 1(a) through the addition of nonlinear feedback (thresholding, gain, and feedback) to a conventional optical vector-matrix multiplier [8] in which the array of LEDs represents the input vector and an array of photodiodes (PD) is used to detect the output vector. The PD array output is thresholded and fed back in parallel to drive the corresponding elements of the LED array. Multi- plication of the input vector by the T_{ij} matrix is achieved by horizontal imaging and vertical smearing of the input vector that is displayed by the LEDs on the plane of the T_{ij} mask. This is implemented by means of an anamorphic lens system omitted from Fig. 1(a) for simplicity. A second

anamorphic lens system (also not shown) is used to collect the light emerging from each row of the T_{ij} mask on individual photo-sites of the PD array. In this scheme a bipolar T_{ij} matrix is realized in incoherent light by dividing each row of the T_{ij} matrix in two subrows, one for positive and one for negative values and bringing the light emerging from each subrow to focus on two adjacent photo-sites of the PD array that are electrically connected in opposition as depicted in Fig. 1. In the system shown in Fig. 1, feedback is achieved by electronic wiring. It is possible and preferable to dispose of electronic wiring altogether and replace it with optical feedback. This can be achieved by combining the PD and LED arrays in a single hybrid or monolithic structure that can also be made to contain all ICs for thresholding, amplification, and driving of LEDs. Optical feedback becomes even more attractive when we consider that arrays of nonlinear optical light amplifiers with internal feedback [9] or optical bi-stability devices (OBDs) [10] can be used to replace the PD/LED array. This can lead to simple compact CAM structure that may be interconnected to perform more sophisticated computations than the nearest neighbor search performed by a single CAM.

The detail and operation of a simple optical system simulating a network of N=32 neurons that is a variation of the scheme presented in Fig. 1 has been reported in [7]. Here we review briefly details of this system that are relevant to the subject matter of this paper.

The systems, details of which are given in Figs. 3-6, was constructed with an array of 32 LEDs and two multichannel silicon PD arrays, each consisting of 32 elements. Twice as many PD elements than LEDs are needed in order to implement a bipolar memory mask transmittance in incoherent light in accordance to the scheme of Fig. 1(b). In this scheme a bipolar binary (BB) T_{ij} mask was utilized. The mask was prepared for M=3 binary state vectors. The three vectors

or words chosen, their Hamming distances from each other, and the resulting T_{ij} memory matrix are reproduced in Fig. 2. The mean Hamming distance between the three vectors is 16. A binary photographic transparency of 32x64 square pixels was computer generated from the T_{ij} matrix by assigning the positive values in any given row of T_{ij} to transparent pixels in one subrow of the mask and the negative values to transparent pixels in the adjacent subrow. To insure that the image of the input LED array is uniformly smeared over the memory mask it was found convenient to split the mask in two halves, as shown in Fig. 3, and to use the resulting submasks in two identical optical arms as shown in Fig. 4. The size of the subrows of the memory submasks was made exactly equal to the element size of the PD arrays in the vertical direction which were placed in register against the masks. Light emerging from each vertically oriented subrow of a memory submask was collected (spatially integrated) by one of the vertically oriented elements of the multichannel PD array. In this fashion the anamorphic optics required in the output part of Fig. 1(a) are disposed of, resulting in a more simple and compact system. Pictorial views of the input LED array and the two submask / PD array assemblies are shown in (a) and (b) of Fig. 5 respectively. All electronic circuits (amplifiers, thresholding comparators, LED drivers etc.) in the 32 parallel feedback channels are contained in the electronic amplification and thresholding box shown in Fig. 4(a) and in the boxes on which the LED array and the two submask / PD array assemblies are mounted (see Fig. 5). A pictorial view of a "composing and display box" is shown in Fig. 6. This contains an arrangement of 32 switches and a 32 element LED display panel whose elements are connected in parallel to the input LED array. The function of this box is to compose and display the binary input word or vector that appears on the input LED array of the system shown in Fig. 5(a).

Once an input vector is selected it appears displayed on the composing box and on the input LED box simultaneously. A single switch is then thrown to release the system into operation with the composed vector as the initializing vector. The final state of the system, the output, appears after a few iterations displayed on the input LED array and display box simultaneously. The above procedure provides for convenient exercising of the system in order to study its response vs. stimulus behavior. An input vector is composed and its Hamming distance from each of the nominal state vectors stored in the memory is noted. The vector is then used to initialize the CAM as described above. The output vector, representing the final state of the CAM which appears almost immediately on the display box, is examined. The response time of the electronic feedback channels, as determined by the 3 dB roll-off of the amplifiers, was about 60 milliseconds. Speed of the operation was not an issue in this study, and thus the slow response time was chosen to facilitate the experiment.

The above implementation of CAM based on the Hopfield model for neural nets indicate the opto-electronic analog of two neurons in synaptic contact shown in Fig. 7. In this scheme the presence of both excitatory and inhibitory synapses require the use of twice the number of neurons implemented in photodetectors and rows of the optical mask in order to realize the bipolar interconnection matrix in incoherent light.

The results of exercising and evaluating the performance of the CAM described above were presented in [7]. These show that the system is capable of associative recall, has error correction capabilities and is extremely robust. It is obvious that considerable simplification can be achieved in the above implementation if a unipolar binary mask is permitted. An immediately obvious advantage of this is that the same number of photodetectors used in the preceding system can be used to implement a CAM with 64 neurons instead 32

with some additional components and a new unipolar binary (UB) mask. For this reason we have carried out a study of methods for implementing CAMs employing unipolar binary T_{ij} matrix which are described in the following sections.

3. CONTENT ADDRESSABLE MEMORY WITH UNIPOLAR BINARY INTERCONNECTION MATRIX

The use of UB interconnection matrix or synaptic mask has the advantage, pointed out earlier, of further simplifying optical implementation of neural networks and of opening the way for the study of larger networks. It also has the advantage of facilitating the use of recyclable spatial light modulators (SLMs) such as the Litton non-volatile magneto-optic SLM (MO-SLM) [11] which is easiest to use as a programmable mask (T_{ij} matrix) in a UB transmission mode. The use of a modifiable, external memory driven, MO-SLM as a T_{ij} mask enables the same CAM to search through a large file of T_{ij} matrices residing in an external store in a relatively short time. With such masks a non-zero threshold level must be adopted as the inhibitory signals to a neuron (or to the pair of photo-diodes in Fig. 7 (b)) arising from negative values of the T_{ij} mask are now absent. Two schemes of adaptive thresholding were examined. One is shown in Fig. 8. In this scheme, suggested by the observation that dormant neurons have a non-zero firing rate, we adopt one half the energy $E = 1/2 \sum_j v_j$ of the UB input vector as a non-zero adaptive thresholding level for the comparator C. The comparator output which can be positive, zero or negative depending on whether the weighted projection $v_i = \sum_j T_{ij} * v_j$ of the input vector is greater, equal or less than E is applied to a zero level thresholding element the output of which is used to drive the corresponding element in the input LED array.

The second scheme examined adds relaxation to the preceding scheme as shown in Fig. 9. As each iteration proceeds in this scheme, the comparator output, the difference between the weighted projection of the current iterate and one half of the energy of the input vector, is attenuated through multiplication by a positive relaxation parameter α of value less than unity. The outcome is added to the value of the previous iterate, retained through the secondary feedback loop with time delay τ and the result is applied to a limiter. Since the initializing input vector has a value of one or zero, the negative value and value of greater than one are clipped while the values between zero and one are remained unchanged through the limiter. The limiter output is used to drive the cor esponding LED in the input LED array. In this fashion a smooth transition of states in the CAM is realized. The technique bears resemblance to the relaxation method used in solution of systems of linear equations.

The results of numerical simulation of the above two schemes, assuming a unipolar binary version of the T_{ij} matrix and three stored vectors are shown in the last two columns of table I. These are compared with the results of simulations for: 1) a grey level mask with zero thresholding, 2) bipolar binary (-1,0,1) mask with zero thresholding, and 3) unipolar binary (0,1) mask with the mean of the projections, $\langle proj \rangle = 1/N \sum_j v_j$, selected as thresholding value. The results are shown in the other columns of table I. The numbers in the table represent the maximum Hamming distance of an input vector chosen to exercise the memory from the stored vector that can be corrected. The exercising input vector is obtained from a stored vector by switching digits from its end. The symbol x in the table means that particular input vector is not recognized even when none of its digits differ from the from the stored vector. The simulations were repeated

for ten sets of randomly formed three vectors for each set a different UB T_{ij} matrix was generated. The results of this exercise are shown in rows of 2-10 of table I. The total sum of errors corrected in each column, i.e. for each of the different combinations of memory masks and thresholding procedures, are shown in the bottom row of table I. The values in this row are taken as a performance measure of the CAMs simulated. The grey level case with zero threshold is taken to represent a relative performance of 100%. This type of CAM was able to correct a total of 246 errors total in the exercise. However, the CAM with the UB mask and input energy thresholding with relaxation is seen have slightly better performance by correcting 260 errors i.e. a relative performance of 105%. Adaptive input energy thresholding (without relaxation) is seen to fare well at 79% relative performance. The poorest in performance was the CAM with UB mask with mean of projections <proj.> as threshold where the relative performance is seen to be 61%.

4. EXPERIMENTAL VERIFICATION

To verify experimentally the performance of the adaptive thresholding schemes of Figs 8 and 9, a modified version of the optical implementation described in section 2 is utilized. In this modified version only one channel of the two arm system of Fig. 4 is utilized. The binary bipolar mask in this arm, which represents one half of the bipolar binary T_{ij} matrix, is replaced by a unipolar binary version of the complete T_{ij} matrix consisting of 32 rows and 32 columns. The 32 columns exactly overlay the elements of the 32 element photo detector (PD) array. For the results reported here the PD array outputs were read by an A/D converter via an analog multiplexer and stored in a DEC 11/23 Modular INstrumentation Computer as illustrated in Fig. 10. The energy of

the input vector is entered in the computer manually as one half the number of elements in the input LED array that are lit. The adaptive thresholding algorithms of Figs. 8 and 9 described in the preceding section are carried out then by the computer which furnishes 32 voltage values for driving the LED array for subsequent iteration. For the adaptive thresholding scheme of Fig. 8, these values, which consist of an array of zeros and ones representing the result of the first iteration, are easily entered in the system manually through the word composer. For the adaptive thresholding and relaxation scheme the computer output consists of an array of numbers each ranging between zero and one for driving the LED array through an appropriate D/A converter. As this interface was not completed at the time of this writing, results for the adaptive thresholding (without relaxation) are included here. A photograph of the computer generated unipolar binary mask employed in the above opto-digital experiment is shown in Fig. 11. It is seen to contain 32 rows and 32 columns as opposed to 32 rows and 64 columns of the bipolar binary mask of Fig. 3 that represented the bipolar binary (-1,0,1) T_{ij} matrix in the first optical implementation [7].

The result of the above opto-digital experiment for the adaptive thresholding (without relaxation) scheme are presented in table II. These show that the CAM with UB mask and adaptive thresholding functions satisfactorily and is capable of recognizing partial inputs of the memory states, i.e. of the three stored vectors, up to 5 errors are tolerated for vector 1, 4 errors for vector 2 and 6 errors for vector 3 for both normal and complement of vectors. The performance is in general agreement with the numerical simulation results presented in table I for this case. Opto-digital experimentation of the type described above is found in our work to be a very useful step in the study of models of neural nets falling

FIGURE CAPTIONS

Fig. 1. Concept for optical implementation of a content addressable memory based on the Hopfield model. (a) matrix vector multiplier incorporating nonlinear electronic feedback, (b) scheme for realizing a binary bipolar memory mask transmittance in incoherent light.

Fig. 2. Stored words, their Hamming distance, and their clipped T_{ij} memory matrix.

Fig. 3. Two halves of T_{ij} memory mask.

Fig. 4. Arrangement for optical implementation of the Hopfield model. (a) Opto-electronic circuit diagram, (b) Pictorial view.

Fig. 5. Views of (a) input LED array and (b) memory submask / PD array assemblies.

Fig. 6. Word composer and display box.

Fig. 7. Two neurons in synaptic contact (a) and their opto-electronic analog (b).

Fig. 8. CAM with unipolar synaptic mask and adaptive thresholding scheme.

Fig. 9. CAM with unipolar synaptic mask and adaptive thresholding with relaxation.

Fig. 10. Experimental opto-digital arrangement used in studying CAM behavior using UB mask and adaptive thresholding and feedback schemes.

Fig. 11. Unipolar Binary T_{ij} memory mask.

Table I. Comparison of different type of memory mask and thresholding procedures (digital simulation).

Table II. Performance of the optical CAM (opto-digital experiment).

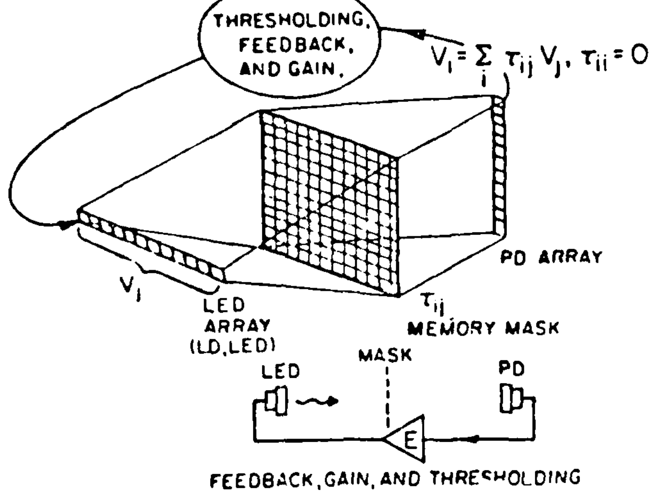

(a)

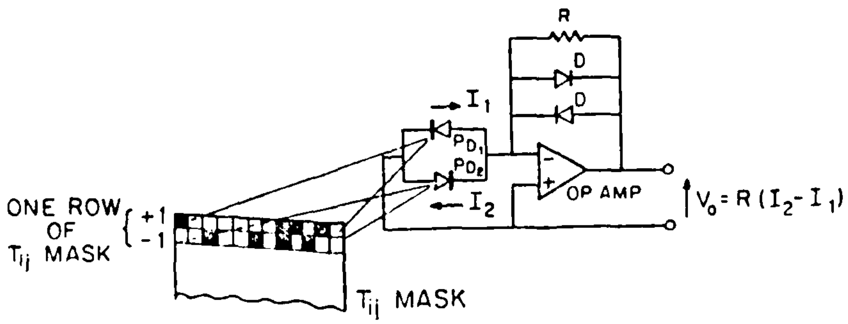

(b)

Fig. 1. Concept for optical implementation of a content addressable memory based on the Hopfield model. (a) matrix vector multiplier incorporating nonlinear electronic feedback. (b) scheme for realizing a binary bipolar memory mask transmittance in incoherent light.

Words to be stored:

Word 1	:	1	1	1	0	0	0	0	1	0	1	0	1	1	1	0	1	1	0	1	1	1	1	0	1	1	0	0	0	0	0	1	0
Word 2	:	0	1	1	0	0	0	0	0	0	0	1	0	0	1	0	1	0	1	0	0	1	1	1	1	0	1	0	1	1	0	1	0
Word 3	:	1	0	1	1	0	0	1	1	1	1	1	1	1	1	1	0	0	0	1	0	1	1	0	0	0	0	1	1	0	0	0	0

Hamming distance from word to word:

	1	2	3
WORD 1	0	15	14
WORD 2	15	0	19
WORD 3	14	19	0

MEMORY or MASK ;

0	-1	1	1	-1	-1	1	1	1	1	-1	1	1	1	1	-1	1	-1	1	1	1	1	-1	-1	1	-1	1	-1	-1	-1	-1	-1
-1	0	1	-1	-1	-1	-1	-1	-1	-1	-1	-1	-1	1	-1	1	1	1	-1	1	1	1	1	1	1	1	-1	-1	1	-1	1	-1
1	1	0	-1	-1	-1	-1	1	-1	1	1	1	1	1	-1	1	-1	-1	1	-1	1	1	-1	1	-1	-1	-1	1	-1	-1	1	-1
1	-1	-1	0	1	1	1	1	1	1	1	1	1	-1	1	-1	-1	-1	1	-1	-1	-1	-1	-1	-1	-1	1	1	-1	1	-1	1
-1	-1	-1	1	0	1	1	-1	1	-1	-1	-1	-1	-1	1	-1	1	1	-1	1	-1	-1	1	-1	1	1	1	-1	1	1	-1	1
-1	-1	-1	1	1	0	1	-1	1	-1	-1	-1	-1	-1	1	-1	1	1	-1	1	-1	-1	1	-1	1	1	1	-1	1	1	-1	1
1	-1	-1	1	1	1	0	1	1	1	1	1	1	-1	1	-1	-1	-1	1	-1	-1	-1	-1	-1	-1	-1	1	1	-1	1	-1	1
1	-1	1	1	-1	-1	1	0	1	1	-1	1	1	1	1	-1	1	-1	1	1	1	1	-1	-1	1	-1	1	-1	-1	-1	-1	-1
1	-1	-1	1	1	1	1	1	0	1	1	1	1	-1	1	-1	-1	-1	1	-1	-1	-1	-1	-1	-1	-1	1	1	-1	1	-1	1
1	-1	1	1	-1	-1	1	1	1	0	-1	1	1	1	1	-1	1	-1	1	1	1	1	-1	-1	1	-1	1	-1	-1	-1	-1	-1
-1	-1	1	1	-1	-1	1	-1	1	-1	0	-1	-1	1	1	-1	-1	1	-1	-1	1	1	1	-1	-1	1	1	1	1	-1	-1	-1
1	-1	1	1	-1	-1	1	1	1	1	-1	0	1	1	1	-1	1	-1	1	1	1	1	-1	-1	1	-1	1	-1	-1	-1	-1	-1
1	-1	1	1	-1	-1	1	1	1	1	-1	1	0	1	1	-1	1	-1	1	1	1	1	-1	-1	1	-1	1	-1	-1	-1	-1	-1
1	1	1	-1	-1	-1	-1	1	-1	1	1	1	1	0	-1	1	-1	-1	1	-1	1	1	-1	1	-1	-1	-1	1	-1	-1	1	-1
1	-1	-1	1	1	1	1	1	1	1	1	1	1	-1	0	-1	-1	-1	1	-1	-1	-1	-1	-1	-1	-1	1	1	-1	1	-1	1
-1	1	1	-1	-1	-1	-1	-1	-1	-1	-1	-1	-1	1	-1	0	1	1	-1	1	1	1	1	1	1	1	-1	-1	1	-1	1	-1
1	1	-1	-1	1	1	-1	1	-1	1	-1	1	1	-1	-1	1	0	-1	1	1	-1	-1	-1	1	1	-1	-1	-1	-1	1	1	1
-1	1	-1	-1	1	1	-1	-1	-1	-1	1	-1	-1	-1	-1	1	-1	0	-1	-1	-1	-1	1	1	-1	1	-1	1	1	1	1	1
1	-1	1	1	-1	-1	1	1	1	1	-1	1	1	1	1	-1	1	-1	0	1	1	1	-1	-1	1	-1	1	-1	-1	-1	-1	-1
1	1	-1	-1	1	1	-1	1	-1	1	-1	1	1	-1	-1	1	1	-1	1	0	-1	-1	-1	1	1	-1	-1	-1	-1	1	1	1
1	1	1	-1	-1	-1	-1	1	-1	1	1	1	1	1	-1	1	-1	-1	1	-1	0	1	-1	1	-1	-1	-1	1	-1	-1	1	-1
1	1	1	-1	-1	-1	-1	1	-1	1	1	1	1	1	-1	1	-1	-1	1	-1	1	0	-1	1	-1	-1	-1	1	-1	-1	1	-1
-1	1	-1	-1	1	1	-1	-1	-1	-1	1	-1	-1	-1	-1	1	-1	1	-1	-1	-1	-1	0	1	-1	1	-1	1	1	1	1	1
-1	1	1	-1	-1	-1	-1	-1	-1	-1	-1	-1	-1	1	-1	1	1	1	-1	1	1	1	1	0	1	1	-1	-1	1	-1	1	-1
1	1	-1	-1	1	1	-1	1	-1	1	-1	1	1	-1	-1	1	1	-1	1	1	-1	-1	-1	1	0	-1	-1	-1	-1	1	1	1
-1	1	-1	-1	1	1	-1	-1	-1	-1	1	-1	-1	-1	-1	1	-1	1	-1	-1	-1	-1	1	1	-1	0	-1	1	1	1	1	1
1	-1	-1	1	1	1	1	1	1	1	1	1	1	-1	1	-1	-1	-1	1	-1	-1	-1	-1	-1	-1	-1	0	1	-1	1	-1	1
-1	-1	1	1	-1	-1	1	-1	1	-1	1	-1	-1	1	1	-1	-1	1	-1	-1	1	1	1	-1	-1	1	1	0	1	-1	-1	-1
-1	1	-1	-1	1	1	-1	-1	-1	-1	1	-1	-1	-1	-1	1	-1	1	-1	-1	-1	-1	1	1	-1	1	-1	1	0	1	1	1
-1	-1	-1	1	1	1	1	-1	1	-1	-1	-1	-1	-1	1	-1	1	1	-1	1	-1	-1	1	-1	1	1	1	-1	1	0	-1	1
-1	1	1	-1	-1	-1	-1	-1	-1	-1	-1	-1	-1	1	-1	1	1	1	-1	1	1	1	1	1	1	1	-1	-1	1	-1	0	-1
-1	-1	-1	1	1	1	1	-1	1	-1	-1	-1	-1	-1	1	-1	1	1	-1	1	-1	-1	1	-1	1	1	1	-1	1	1	-1	0

Fig. 2. Stored words, their Hamming distance, and their clipped Bipolar binary (BB) T memory matrix.

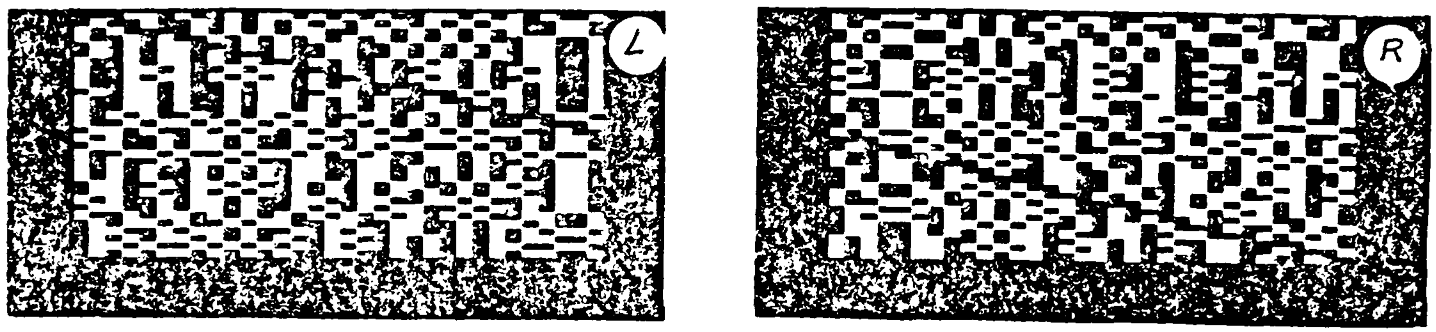

Fig. 3. Two halves of Bipolar binary T_{ij} memory mask.

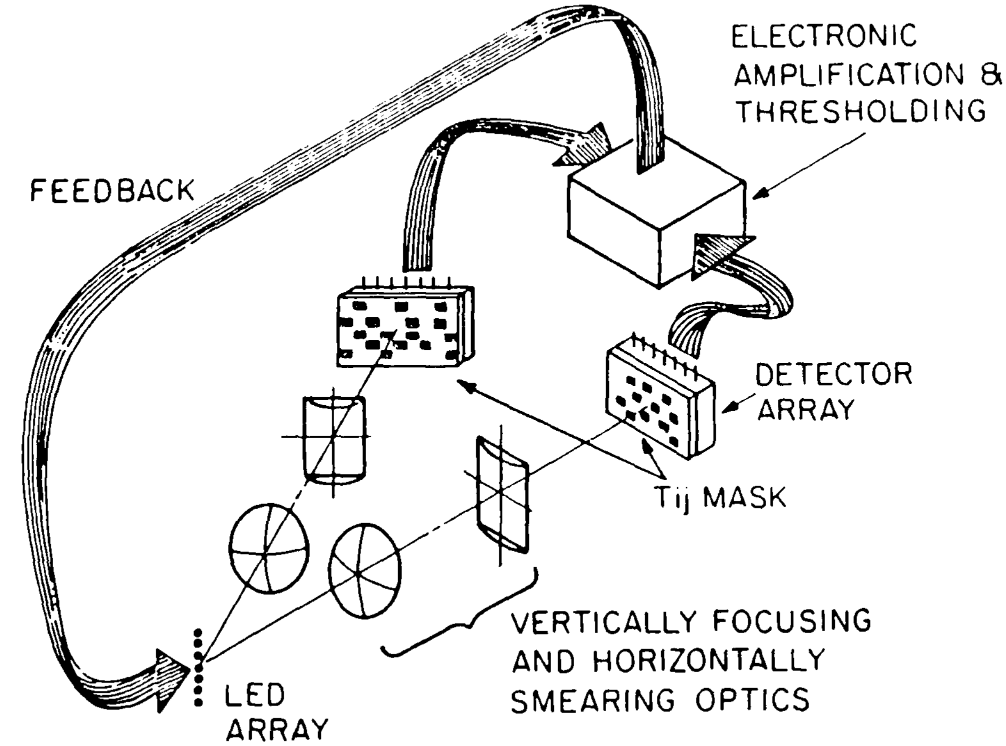

(a)

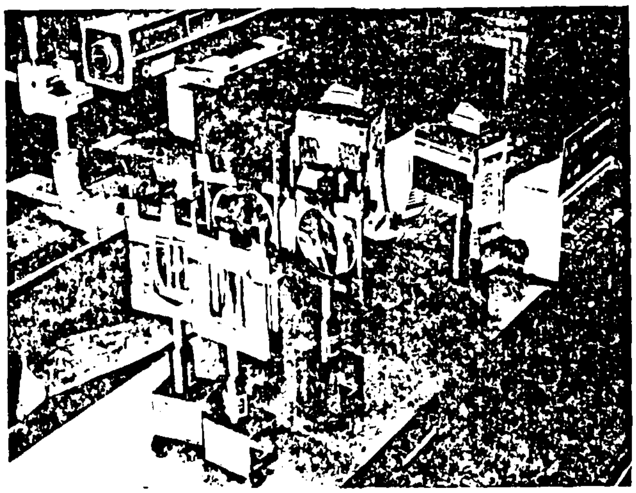

(b)

Fig. 4. Arrangement for optical implementation of the Hopfield model.
(a) Opto-electronic circuit.

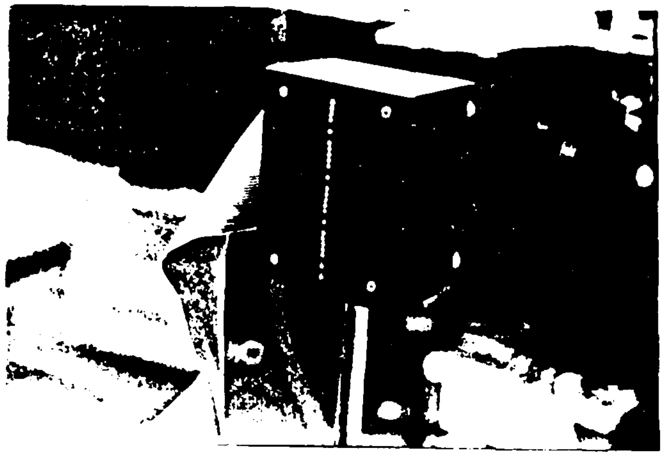

(a)

(b)

Fig. 5. Views of input LED array (a) and memory submask/PD array assemblies (b).

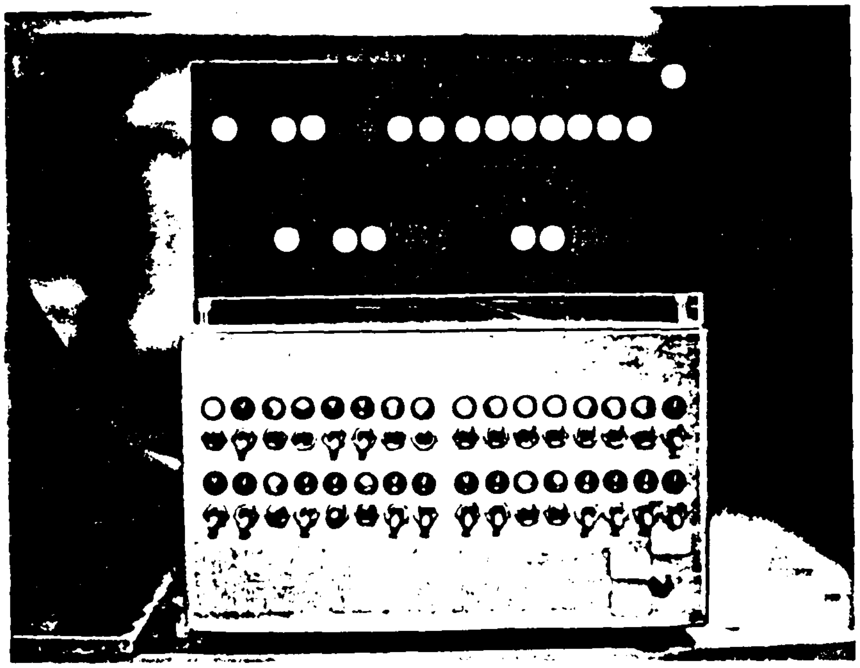

Fig. 6. Word composer and display box.

From: R. Restak THE BRAIN,
Bantam (1984).

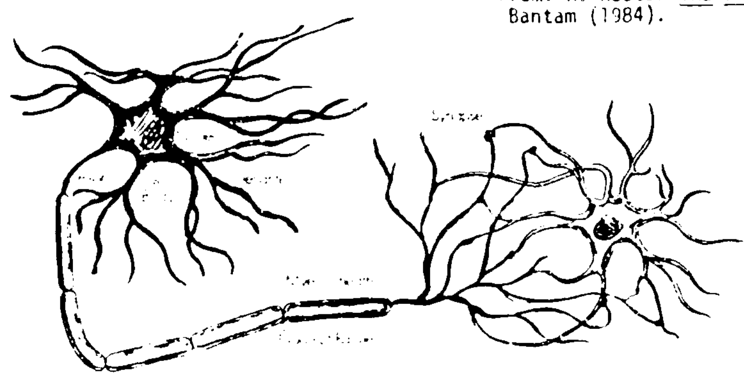

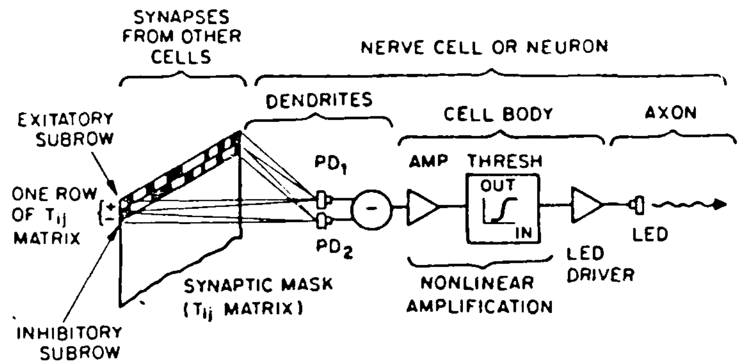

Fig. 7. Two neurons in synaptic contact (a) and their opto-electronic analog (b).

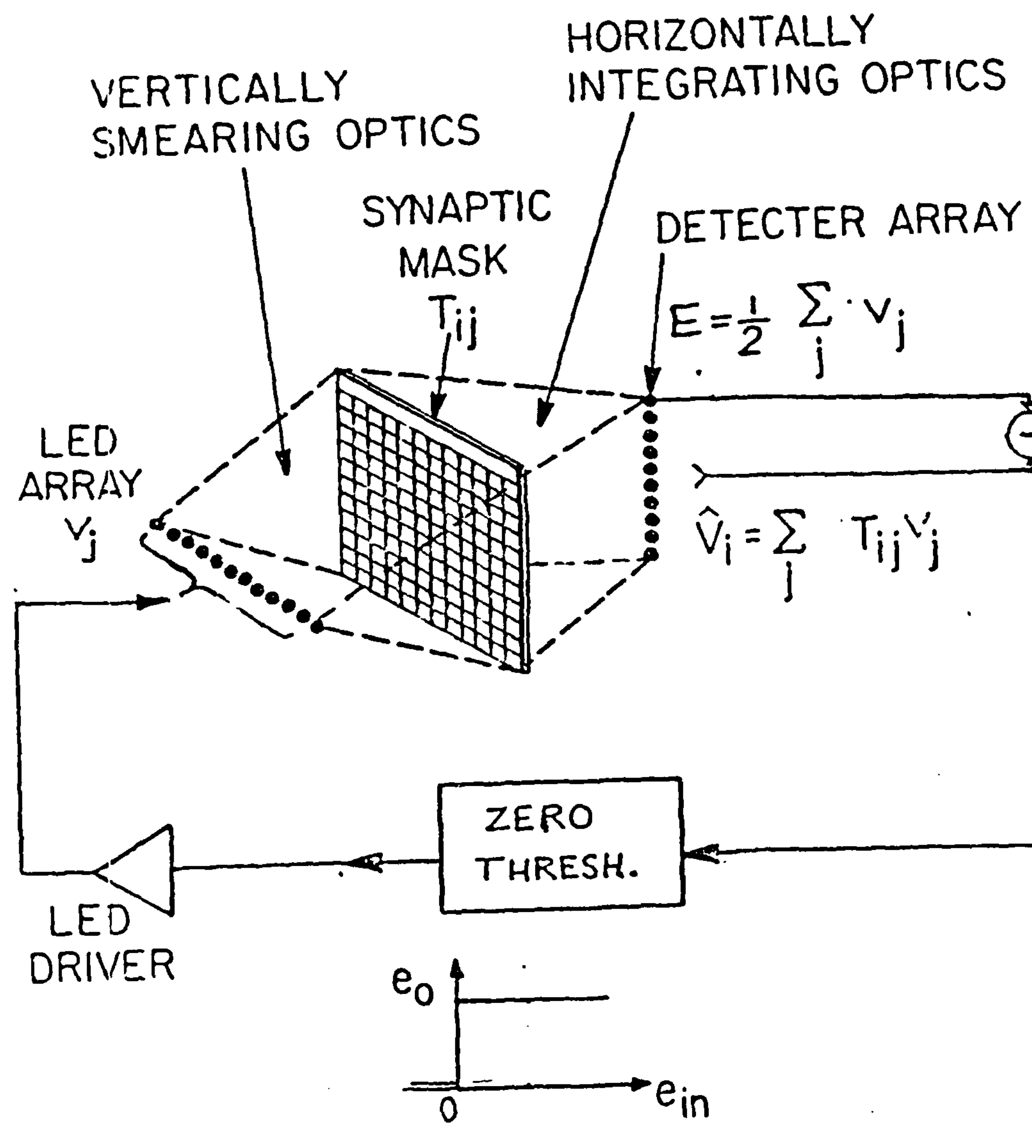

Fig. 8. CAM with unipolar synaptic mask and adaptive thresholding scheme.

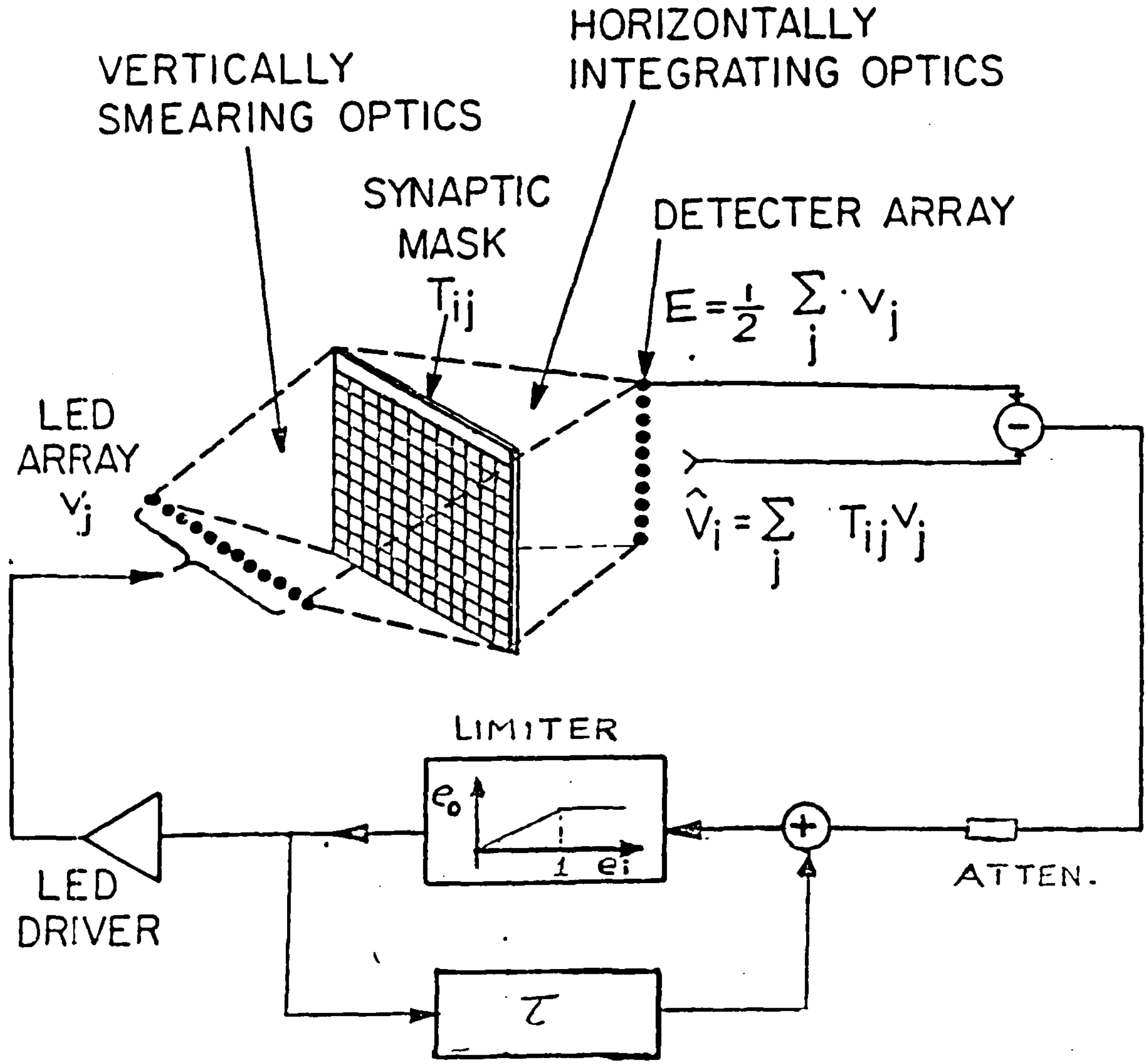

Fig. 9. CAM with unipolar synaptic mask and adaptive thresholding with relaxation.

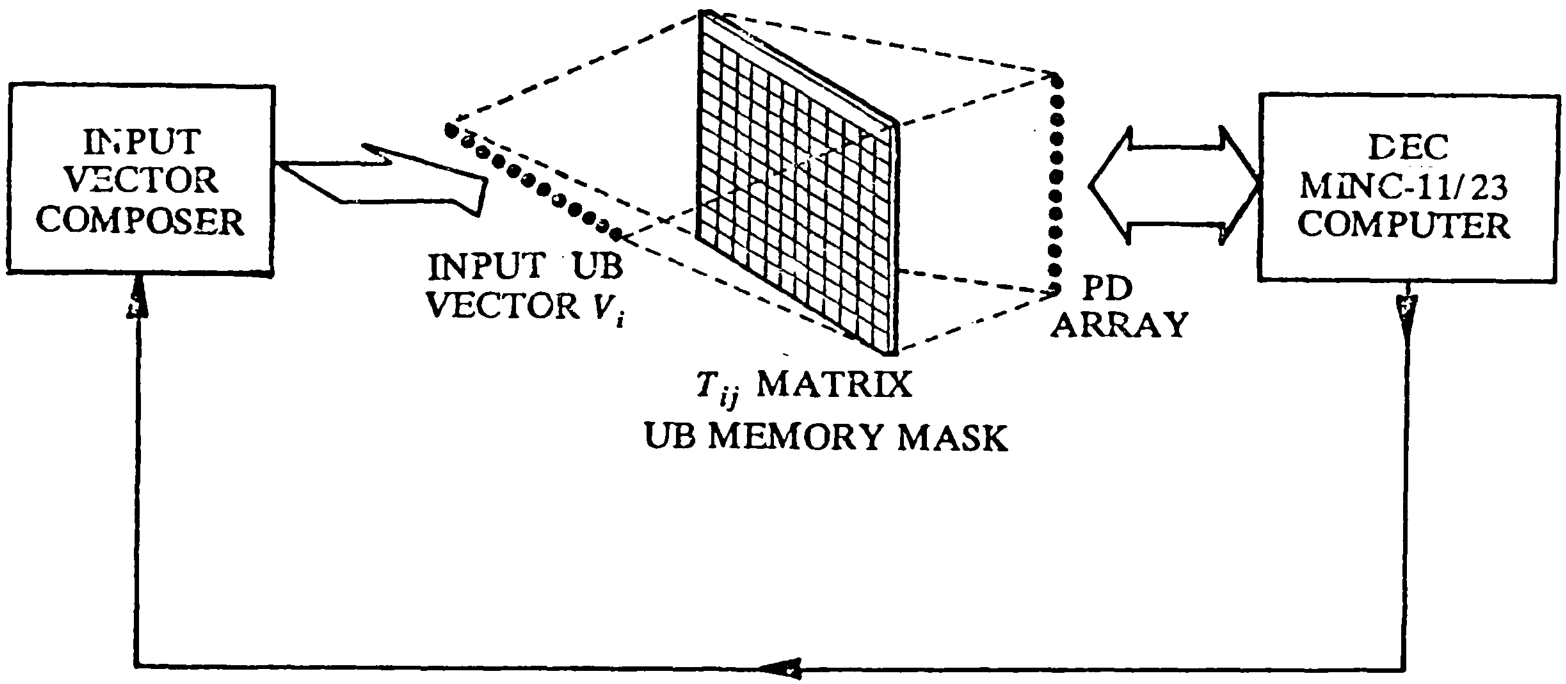

Fig. 10. Experimental opto-digital arrangement used in studying CAM behavior using UB mask and adaptive thresholding and feedback schemes.

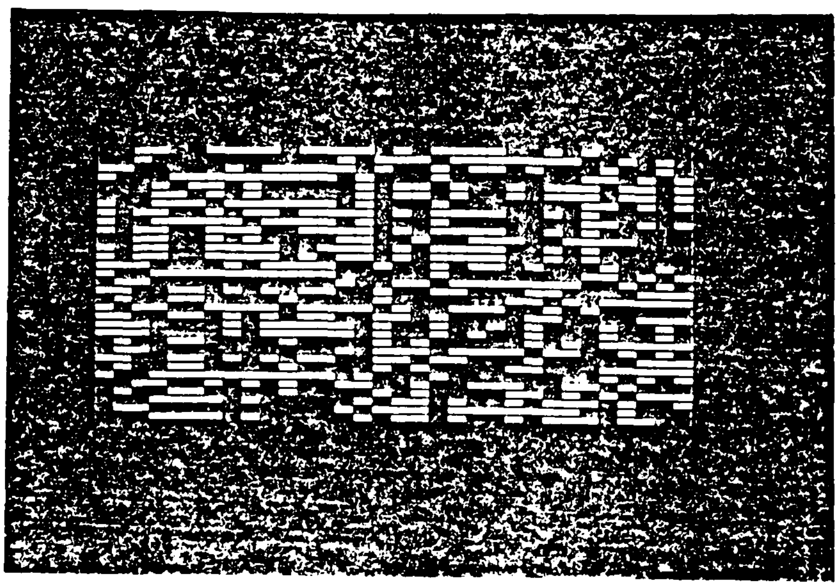

Fig. 11. Unipolar Binary T_{ij} memory mask.

Set	vector	Memory Mask/Thresholding Value				
		Grey/zero	(1,0-1)/zero	$(1,0)/\langle\text{proj.}\rangle$	$(1,0)/\langle E_{in}\rangle$	$(1,0)/\langle E_{in}\rangle$ & relaxation
1	1	11	10	x	15	11
	2	2	2	1	2	3
	3	12	10	8	9	11
2	1	19	17	15	16	19
	2	2	2	x	0	12
	3	4	8	0	1	11
3	1	9	10	10	10	10
	2	10	10	14	14	10
	3	10	9	8	9	10
4	1	0	x	x	x	0
	2	2	2	1	2	3
	3	0	x	x	x	0
5	1	9	10	10	9	10
	2	8	4	2	4	8
	3	12	13	12	13	13
6	1	6	4	1	6	7
	2	8	x	x	x	8
	3	10	8	6	7	11
7	1	6	6	3	3	7
	2	6	2	x	2	3
	3	9	7	7	7	9
8	1	13	13	13	13	13
	2	11	11	7	9	12
	3	7	1	0	0	4
9	1	3	x	x	x	1
	2	15	16	17	16	15
	3	10	11	6	9	10
10	1	13	6	x	5	11
	2	9	10	10	10	11
	3	10	5	x	4	7
Sum of errors corrected		246	207	151	195	260
Relative Performance in percent		100	84	61	79	105

Table I. Comparison of different types of memory mask and thresholding procedures (Numerical simulation).

D_h	Recognized Vector (m=1)			Recognized Vector (m=2)			Recognized Vector (m=3)		
	Opto-digital Experiment	UB/without relaxation (simulation)	UB/with relaxation simulation	Opto-digital Experiment	UB/without relaxation (simulation)	UB/with relaxation (simulation)	Opto-digital Experiment	UB/without relaxation (simulation)	UB/with relaxation (simulation)
0	1	1	1	2	2	2	3	3	3
1	1	1	1	2	2	2	3	3	3
2	1	1	1	2	2	2	3	3	3
3	1	1	1	2	2	2	3	3	3
4	1	1	1	2	2	2	3	3	3
5	1	1	1	OSC	2	2	3	3	3
6	OSC	1	1	OSC	2	2	3	3	3
7	OSC	1	1	OSC	2	2	OSC	3	3
8	OSC	1	1	OSC	2	2	OSC	3	3
9	OSC	1	1	OSC	2	2	OSC	3	3
10	OSC	1	1	OSC	2	2	OSC	3	3
11	OSC	1	1	OSC	2	2	OSC	3	3
12	OSC	3	1	OSC	OSC	OSC	OSC	3	3
13	OSC	3	OSC	OSC	(3)	(3)	OSC	(2)	(2)
14	OSC	OSC	1	OSC	OSC	(3)	OSC	(2)	(2)
15	OSC	OSC	1	1	1	1	OSC	(2)	(2)
16	OSC	OSC	1	1	1	1	OSC	3	(2)
17	OSC	OSC	3	OSC	3	1	OSC	(2)	(2)
18	OSC	(2)	3	OSC	(2)	(2)	OSC	3	OSC
19	OSC	(2)	(2)	OSC	(2)	(2)	OSC	(2)	(2)
20	OSC	(2)	(1)	OSC	(2)	(2)	OSC	(2)	(2)
21	OSC	(1)	(1)	OSC	(2)	(2)	OSC	(3)	(3)
22	OSC	(1)	(1)	OSC	(2)	(2)	OSC	OSC	(3)
23	OSC	(1)	(1)	OSC	(2)	(2)	OSC	(3)	(3)
24	OSC	(1)	(1)	OSC	(2)	(2)	OSC	(3)	(3)
25	OSC	(1)	(1)	OSC	(2)	(2)	(3)	(3)	(3)
26	(1)	(1)	(1)	OSC	(2)	(2)	(3)	(3)	(3)
27	(1)	(1)	(1)	(2)	(2)	(2)	(3)	(3)	(3)
28	(1)	(1)	(1)	(2)	(2)	(2)	(3)	(3)	(3)
29	(1)	(1)	(1)	(2)	(2)	(2)	(3)	(3)	(3)
30	(1)	(1)	(1)	(2)	(2)	(2)	(3)	(3)	(3)
31	(1)	(1)	(1)	(2)	(2)	(2)	(3)	(3)	(3)
32	(1)	(1)	(1)	(2)	(2)	(2)	(3)	(3)	(3)

*D_h : Hamming Distance of an initializing vector from $b_i^{(m)}$

*( ) denotes complement of vectors

*OSC: oscillates between the states

Table II. Performance of the optical CAM with Adaptive Energy Thresholding (no relaxation) (Results of opto-digital experiment).

APPENDIX II

OPTICAL ANALOGS OF TWO-DIMENSIONAL NEURAL NETWORKS AND THEIR APPLICATION IN RECOGNITION OF RADAR TARGETS

N.H. Farhat, S. Miyahara and K.S. Lee
University of Pennsylvania
The Electro-Optics and Microwave-Optics Laboratory
200 S. 33rd Street
Philadelphia, PA 19104-6390

ABSTRACT

Optical analogs of 2-D distribution of idealized neurons (2-D neural net) based on partitioning of the resulting 4-D connectivity matrix are discussed. These are desirable because of compatibility with 2-D feature spaces and ability to realize denser networks. An example of their use with sinogram classifiers derived from realistic radar data of scale models of three aerospace objects taken as learning set is given. Super-resolved recognition from partial information that can be as low as 20% of the sinogram data is demonstrated together with a capacity for error correction and generalization.

INTRODUCTION

Neural net models and their analogs furnish a new approach to signal processing that is collective, robust, and fault tolerant. Optical implementations of neural nets[1,2] are attractive because of the inherent parallelism and massive interconnection capabilities provided by optics and because of emergent optical technologies that promise high resolution and high speed programmable spatial light modulators (SLMs) and arrays of optical bistability devices (optical decision making elements) that can facilitate the implementation and study of large networks. Optical implementation of a one-dimensional network of 32 neurons exhibiting robust content-addressability and associative recall has already been demonstrated to illustrate the above advantages.[3] Extension to two-dimensional arrangements are of interest because these are suitable for processing of 2-D image data or image classifiers directly and offer a way for optical implementation of large networks.[4]

In this paper we will discuss content addressable memory (CAM) architectures based on partitioning of the four dimensional $T_{ijk\ell}$ memory or interconnection matrix encountered in the storage of 2-D entities. A specific architecture and implementation based on the use of partitioned unipolar binary (u.b.) memory matrix and the use of adaptive thresholding in the feedback loop are described. The use of u.b. memory masks greatly simplifies optical implementations and facilitates the realization of larger networks $\sim(10^3-10^4$ neurons). Numerical simulations showing the use of such 2-D networks in the recognition of dilute point-like objects that arise in radar and other similar remote sensing imaging applications are described. Dilute objects pose a problem for CAM storage because of the small

Hamming distance between them. Here we show that coding in the form of a *sinogram classifier* of the dilute object can remove this limitation permitting recognition from partial versions of the stored entities. The advantage of this capability in super-resolved recognition of radar targets is discussed in the context of a new type of radar diversity imaging, studied extensively in our laboratory, that is capable of providing sinogram information compatible with 2-D CAM storage and interrogation. Super-resolved automated recognition of scale models of three aero-space objects from partial information as low as 20% of a learned entity is shown employing hetero-associative storage where the outcome is a word label describing the recognized object. Capacity for error correction and generalization were also observed.

TWO-DIMENSIONAL NEURAL NETS

Storage and readout of 2-D entities in a content addressable or associative memory is described next. Given a set of M 2-D bipolar binary patterns or entities $v_{ij}^{(m)}$ m=1,2...M each of NxN elements represented by a matrix of rank N, these can be stored in a manner that is a direct extension of the 1-D case as follows: For each element of a matrix a new NxN matrix is formed by multiplying the value of the element by all elements of the matrix including itself taking the self product as zero. The outcome is a new set of N^2 binary bipolar matrices each of rank N. A formal description of this operation is,

$$T_{ijk\ell}^{(m)} = \begin{cases} v_{ij}^{(m)} \, v_{k\ell}^{(m)} & \\ 0 & i=k,\ j=\ell \end{cases} \tag{1}$$

which is a four dimensional matrix. An overall or composite synaptic or connectivity memory matrix is formed then by adding all 4-D matrices $T_{ijk\ell}^{(m)}$ i.e.,

$$T_{ijk\ell} = \sum_m T_{ijk\ell}^{(m)} \tag{2}$$

This symmetric 4-D matrix has elements that vary in value between -M to M also in steps of two as for the 1-D neural net case and which assume values of +1 and -1 (and zeros for the self product elements) when the matrix is clipped or binarized as is usually preferable for optical implementations. Two dimensional unipolar binary entities $b_{ij}^{(m)}$ are frequently of practical importance. These can be transformed in the usual way into bipolar binary matrices through $v_{ij}^{(m)} = (2b_{ij}^{(m)} - 1)$ which are then used to form the 4-D connectivity matrix or memory as described. Also, as in the 1-D neural net case, the prompting entity can be unipolar binary $b_{ij}^{(m)}$, which would simplify further optical

implementations in incoherent light.

Architectures for optical implementation of 2-D neural nets must contend with the task of realizing a 4-D memory matrix. Here a scheme is presented that is based on the partitioning of the 4-D memory matrix into an array of 2-D matrices of rank N.

Nearest neighbor search of the memory matrix for a given entity $b_{ij}^{(mo)}$ is done by forming the estimate,

$$\hat{b}_{ij}^{(mo)} = \sum_{k,\ell}^{N} T_{ijk\ell}\, b_{k\ell}^{(mo)} \quad \ldots\ldots \; i,j,k,\ell = 1,2,\ldots N \tag{3}$$

followed by thresholding to obtain a new u.b. matrix which is used to replace $b_{k\ell}^{(mo)}$ in eq. (3) and the procedure is repeated until the resulting matrix converges to the stored entity closest to the initiating matrix $b_{ij}^{(mo)}$. The operation in eq. (3) can be interpreted as first partitioning of the 4-D $T_{ijk\ell}$ matrix into an array of 2-D submatrices of rank N: $T_{11k\ell}$, $T_{12k\ell}$, ..., $T_{1Nk\ell}$; $T_{21k\ell}$, $T_{22k\ell}$, ..., $T_{2Nk\ell}$; ..., $T_{N1k\ell}$, $T_{N2k\ell}$, ..., $T_{NNk\ell}$ as depicted schematically in Fig. 1(a) where the partition submatrices are arranged in a 2-D array. This first step is followed by multiplication of $b_{k\ell}^{(mo)}$ by each of the partition submatrices, on an element by element basis, and summing the products for each submatrix to obtain the first estimate $\hat{b}_{ij}^{(mo)}$. The tensor multiplications and summation operations called for in eq. (3) are carried out in Fig. 1(a) by placing a spatially integrating photodetector (PD) behind each submatrix of the partitioned

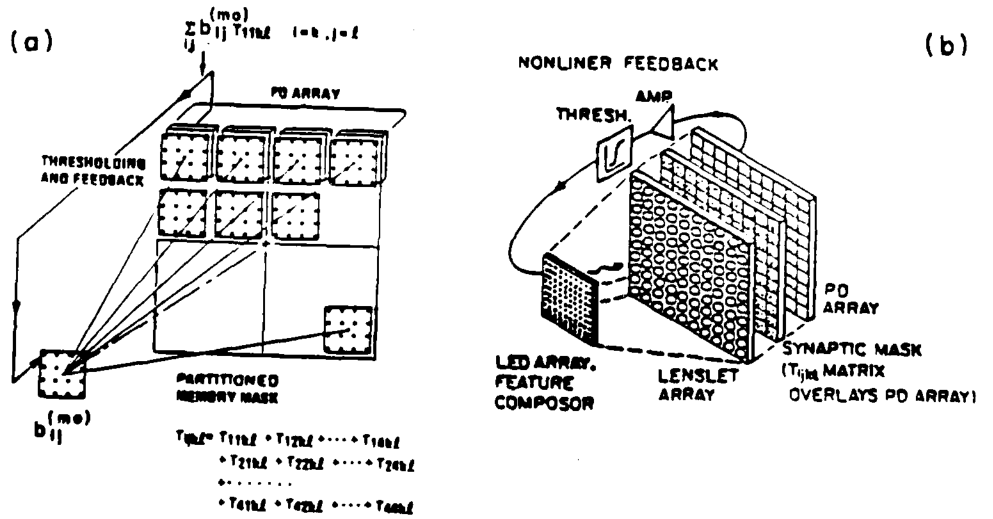

Fig. 1. Optical analog of 2-D neural net. (a) Architecture based on partitioning of connectivity matrix, (b) Opto-electronic embodiment.

memory mask which is assumed for the time being to be realized by pixel transmittance modulation in an ideal transparency capable of assuming negative transmittance values. The input entity $b_{ij}^{(mo)}$ is assumed to be displayed on a suitable LED array. The LED display of $b_{ij}^{(mo)}$ is multiplied by the ideal transmittance of each of the partition submatrices by imaging the display on each of these with exact registration of pixels by means of a lenslet array as depicted in Fig. 1(b). The output of each PD, proportional to one of the components of eq. 3, is thresholded, amplified, and fed back to drive an associated LED. The (i,j)-th LED is paired with the (i,j)-th PD. This completes the interconnection of the 2-D array of NxN neurons in the above architecture where each neuron communicates its state to all other neurons through a prescribed four dimensional synaptic or memory matrix in which information about M 2-D binary matrices of rank N (entities) have been stored distributively. The number of 2-D entities that can be stored in this fashion is $M \simeq N^2/8\ell nN$, which follows directly from the storage capacity formula for the 1-D neural net case by replacing N by N^2.

The added complexity associated with having to realize a bipolar transmittance in the partitioned $T_{ijk\ell}$ memory mask of Fig. 1 can be avoided by using unipolar transmittance. This can lead however to some degradation in performance. A systematic numerical simulation study[5] of a neural net CAM in which statistical evaluation of the performance of the CAM for various types of memory masks (multivalued, clipped ternary, clipped u.b.) and thresholding schemes (zero threshold, adaptive threshold where energy of input vector is used as threshold, adaptive thresholding and relaxation) was carried out. The results indicate that a u.b. memory mask can be used with virtually no sacrifice in CAM performance when the adaptive thresholding and relaxation scheme is applied. The scheme assumes an adaptive threshold is used that is proportional to the energy (total light intensity) of the input entity displayed by the LED array at any time. In the scheme of Fig. 1(b) this can be realized by projecting an image of the input pattern directly onto an additional PD element. The PD output being proportional to the total intensity of the input display is used as a variable or adaptive threshold in a comparator against which the outputs of the PD elements positioned behind the partitioned components of the $T_{ijk\ell}$ memory mask are compared. The outcomes, now bipolar, are attenuated and each is fed into a limiting amplifier with delayed feedback (relaxation). Each limiter/amplifier output is used to drive the LED that each photodetector is paired with. It was found[5] that this scheme yields performance equivalent to that of an ideal CAM with multivalued connectivity matrix and zero thresholding. Note that although the initializaing 2-D entity $b_{ij}^{(mo)}$ is unipolar binary, the entities fed back after adaptive thresholding and limited amplification to drive the LED array would initially be analog resulting in multivalued iterates and intensity displays. However, after few iterations the

outputs become binary assuming the extreme values of the limiter. The ability to use u.b. memory matrices in the fashion described means that simple black and white photographic transparencies or binary SLMs can be used respectively as stationary or programmable synaptic connectivity masks as suggested by Fig. 1.

SINOGRAM CLASSIFIERS AND HETEROASSOCIATIVE STORAGE

Sinograms are object representations encountered in tomography[6,7]. They are also useful as object classifiers specially when the objects are point-like and dilute[8]. Given a set of 2-D dilute objects the Hamming distances between their sinogram classifiers will be greater than the Hamming distances between the objects themselves, with both sets digitized to the same number of pixels, making it easier for an associative memory to distinguish between the sinograms[8]. Sinogram classifiers have additional advantages that enable scale, rotation, and shift invariant recognition of radar target which can not be detailed here because of limited space. A sinogram is a cartesian plot of the polar projections of object detail. For example referring to Fig. 2(a) which represents a dilute object consisting of 16 points on a 32x32 pixel grid, the distance that the projection of each point makes on the y axis as measured from the origin when the object is rotated about the origin traces a sinusoidal pattern when plotted against rotation angle as shown in Fig. 2(b). Figure 2(c) is a

(a) (b) (c) (d)

Fig. 2. Sinogram generation. (a) Sparse object, (b) Sinogram, (c) Digitized sinogram, (d) Experimental sinogram generation in radar by range-profile measurement.

digitized version of the sinogram of Fig. 2(b) plotted on a 32x32 pixel grid. The sinogram of a radar target is produced by measuring the differential range or range-profile of the target employing the arrangement of Fig. 2(d). The system basically measures, with high resolution, the differential distance (differential range or range-profile) from the rotation center of the projections of the scattering centers of the object (here scale models of aerospace targets) on the line-of-sight or the radar system. Cartesian plots of the differential distance of range-profile versus azimuthal angle of rotation ϕ results in a sinogram classifier or feature space of the target which characterizes it at any fixed elevation angle θ. The top row of Fig. 3 shows three digitized sinogram classifiers of scale models of three aerospace targets plotted on a 32x32 pixel

grid. These are treated as a learning set and stored hetero-associatively rather than autoassociatively be replacing $v_{k\ell}^{(m)}$ in eq. (1) by $r_{k\ell}^{(m)}$ $k,\ell=1,2...32$; $m=1,2,3$ where $r_{k\ell}^{(m)}$ represents abbreviated word labels shown in the bottom row of Fig. 3 with which the three test objects are to be associated.

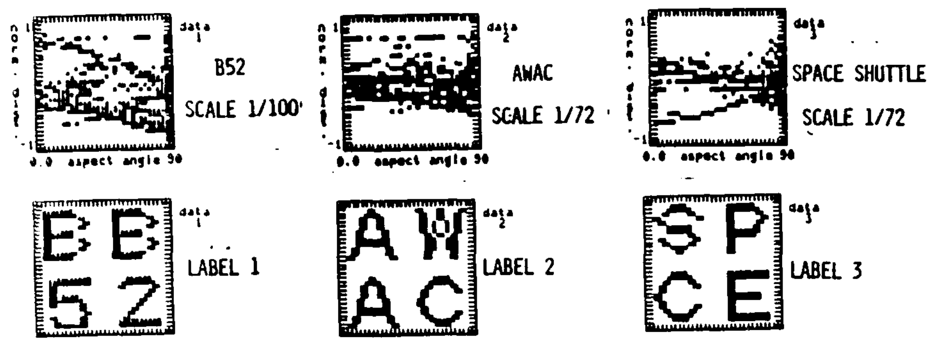

Fig. 3. Hetero-associative storage. Digitized sinograms (top) and associated word labels (bottom).

RESULTS

Representative results of numerical simulation of exercising the heteroassociative memory matrix with complete and partial versions of one of the stored entities in which the fraction η of correct bits or pixels in the partial versions ranged between 1 and .1 are presented in Fig. 4. Reliable recognition was found to occur following one iteration for all entities stored down to η = .2. For η = .1 or less successful recall of correct labels was found to depend on the angular location of the partial data the memory is presented with as illustrated in the two

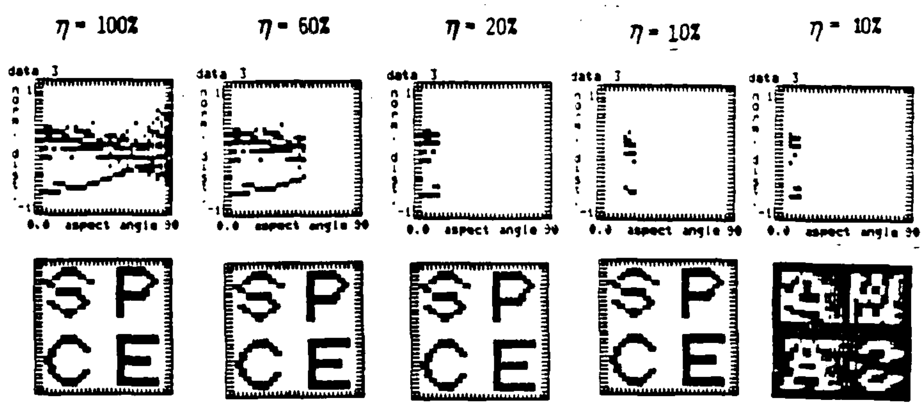

Fig. 4. Example of recognition from partial information. Complete and partial sinograms of data set 3 used as input (top), and final memory state-recognized label (bottom).

right-most examples in Fig. 4. Here the memory could not label the partial input correctly but converged instead onto a label that it did not learn before. This appears to be a generalization (mixture) of the three entities stored earlier. This is quite analogous to the generalization capability of the brain. Note the generalization is contrast reversed as we know that stable states of a memory with symmetric connectivity matrix are not only the entities stored but also their compliments.

CONCLUSIONS

Architectures for optical implementation of 2-D neural nets based on partitioning of the 4-D connectivity matrix are shown to be suitable for use with 2-D object classifiers or feature spaces. An example of their utility in super-resolved recognition (labeling) of radar targets characterized by sinogram classifiers is presented. The results show that neural net models and their opto-electronic analogs furnish a new viable approach to signal processing that is both robust and fault tolerant.

ACKNOWLEDGEMENT

The work described was carried out under a grant from DARPA/NRL, and partial support from AFOSR, ARO, and RCA (GE) Corporation.

REFERENCES

1. D. Psaltis and N. Farhat, Opt. Lett., 10, 98, (1985).
2. A.D. Fisher, et. al., SPIE, 625, 28 (1986).
3. N. Farhat, D. Psaltis, A. Prata and E. Paek, App. Optics, 24, 1469, (1985).
4. N. Farhat and D. Psaltis, Digest OSA Annual Meeting, Wash., D.C., p. 58, (1985).
5. K.S. Lee and N. Farhat, Digest OSA Annual Meeting, Wash., D.C., p. 48, (1985).
6. G. Herman, Image Reconstruction From Projections (Academic Press, N.Y., 1980), p. 11.
7. G.R. Gindi and A.F. Gmitro, Opt. Eng., 23, p. 499, (1984).
8. N. Farhat and S. Miyahara, Technical Digest, Spring 86 OSA Topical Meeting on Signal Recovery and Synthesis II, p. 120, (1986).

APPENDIX III

Phased Array Antenna Pattern Synthesis

By Simulated Annealing

N. Farhat and B. Bai
University of Pennsylvania
The Moore School of Electrical Engineeing
Electro-Optics And Microwave Optics Laboratory
Philadelphia, PA 19104

ABSTRACT: A new procedure is described for optimum phased array synthesis. The synthesis is optimized by a simulated annealing process in which the energy function is directly related to the far field intensity of a phased array. Numerical simulation results are presented. A possible optical-digital hybrid implementation that can perform the required computation at higher speed than a pure digital implementation is discussed.

1. INTRODUCTION

For the synthesis of an antenna array with uniformly spaced elements, it is well known that, if the current distribution function is not restricted, a Dolph-Chebyshev distribution function over the antenna gives rise to an optimum pattern which has the lowest sidelobe level for a specified mainbeam width[1]. However, if for the purpose of easy practical implementation, the distribution function is restricted to some specific set, other methods have to be investigated and used for optimum synthesis. The simulated annealing method presented here is, by our study, one of the choices for optimum synthesis of phased arrays with restricted distribution functions. The synthesis is optimal in the sense that the lowest sidelobe level is achieved while the specified mainbeam width is maintained. This method can be used for both microwave phased arrays and optical

arrays. In our study so far, we have been mainly concerned with optical arrays, which appear to be technologically feasible with the present electronic and optical technologies. Hence, the parameters assumed in the simulations below are relevant to the optical case, but the method and conclusion apply to phased arrays in general.

2. SIMULATED ANNEALING METHOD

Metropolis et al. introduced the simulated annealing algorithm for calculating the properties of any substance of interacting individual molecules[2]. The algorithm was previously applied to some optimization problems, including physical design of computers, and the traveling salesmn problem[3]. The method can be extended for general optimization problems. For the system to be optimized, an "energy" function E is first established and a dynamic variable T, the "temperature" of the system, is chosen to control the process. Starting at a high "temperature", the system is slowly cooled down, until the system "freezes" and reaches the optimum state in a manner similar to annealing of a crystal during growth to reach a near perfect structure. At each "temperature", a change in the system is made according to a certain rule, and then the "energy" change of the system ΔE is calculated. If $\Delta E<0$, the system alteration is retained and the process is continued. The acceptance or rejection of the alteration or change of grain of the system when $\Delta E>0$ is treated probabilistically. Accordingly, the Boltzman factor $f(\Delta E)=exp(-\Delta E/KT)$ is calculated, where K is a constant whose dimension depends on the dimensions of ΔE and T. Then a random number R uniformly distributed in the intervial [0,1) is chosen. If $R<f(\Delta E)$, the change of grain is

retained; on the other hand, if $R > f(\Delta E)$, the change is discarded, that is, the system before change is used for the next step of the process. This procedure is repeated for each "temperature" until the system is optimized to reach a global energy minimum. The choices of K and the initial T are crucial for the success and speed of convergence of simulated annealing process. Because of the probabilistic Boltzman selection rule of the $\Delta E > 0$ case, the process can always get out of a local minimum of the "energy" function in which it could get trapped and proceed to the desired global minimum. This makes simulated annealing different from iterative improvement procedure[3]-[6].

3. ANALYTICAL CONSIDERATIONS

For a 2-dimensional phased array with (2M+1) (2N+1) identical subapertures(elements), the array function can be expressed as[7],

$$g(\xi,\eta) = \sum_{m=-M}^{M} \sum_{n=-N}^{N} W_{mn}\, t(\xi,\eta) * \delta(\xi - mA, \eta - nB) \qquad (1)$$

where, A is the spacing between elements in ξ direction and B in η direction; W_{mn} is a complex quantity and represents the amplitude and phase modulation of the (m,n)th subaperture; $t(\xi,\eta)$ is the subaperture function and is the same for all the subapertures; the symbol '*' stands for convolution.

The scalarized far field pattern G(fx,fy) of a phased array is proportional to the Fourier transform (Fraunhofer pattern) of its array function $g(\xi,\eta)$[7]. Therefore, if the proportionality constant is ignored, the far field can be expressed as,

$$G(f_x, f_y) = \mathfrak{F}[g(\xi,\eta)]$$

$$= \mathfrak{F}[t(\xi,\eta)] \sum_{m=-M}^{M} \sum_{n=-N}^{N} W_{mn} \exp[-j2\pi(mAf_x + nBf_y)] \qquad (2)$$

where, $\mathfrak{F}[\cdot]$ designates Fourier transform and $fx = \frac{x}{\lambda R_0}$, and $fy = \frac{y}{\lambda R_0}$; λ is the wavelength; x, y, and RO are shown in the diffraction geometry in Fig.1. We assume a uniform subaperture function, that is,

$$t(\xi,\eta) = \begin{cases} 1 & |\xi| < \frac{a}{2},\ |\eta| < \frac{b}{2} \\ 0 & \text{otherwise} \end{cases} \qquad (3)$$

where, a and b are the subaperture dimensions in ξ and η directions, respectively. The Fourier transform of $t(\xi,\eta)$ (the subaperture factor) is,

$$T(f_x, f_y) = \frac{\sin \pi a f_x}{\pi f_x} = a\,\mathrm{sinc}(\pi a f_x) \qquad (4)$$

where,

$$\mathrm{sinc}(x) = \frac{\sin x}{x}$$

The double summation term in (2)

$$A(f_x, f_y) = \sum_{m=-M}^{M} \sum_{n=-N}^{N} W_{mn} \exp[-j2\pi(mAf_x + nBf_y)] \qquad (5)$$

is the usual array factor.

Since T(fx,fy) is fixed for the given subaperture function and it varies much more slowly than the array factor, the effect of the subaperture factor is insignificant in the present synthesis. The array factor A(fx,fy) will be studied by changing the weighting factor

W_{mn} for all possible m and n to achieve the optimum radiation pattern.

The "energy" function in simualted annealing can be established in many different ways for phased array synthesis. Since our primary work is done for optical and infrared phased arrays and this kind of arrays has a relatively large size compared to the wavelength λ used (λ on th order of 10^{-6} m), the beam width is very small (on the order of 10^{-2} degrees). It is important to achieve the lowest sidelobe level. For this purpose, one obvious way to choose the "energy" function for phased array synthesis would be the energy outside a specified main lobe. When this energy function is minimized, if the total energy remains constant, it could be expected that the energy would become concentrated in the main beam. Consequentely, the relative sidelobe level could be minimized. But, from simulations that we have run, it turns out that this energy function cannot minimize the sidelobe level. This is understandable, if one recalls the pattern given by the Dolph-Chebyshev distribution, that instead of concentrating in the main beam, the energy has the tendency to distribute itself equally among all the side lobes as the sidelobe level is optimized. This does not mean that the energy in the side lobes is minimized. In the simulation presented here, the intensity E associated with the highest sidelobe level is used as the "energy" function for simulated annealing. Of course, if necessary, a constraint about the beamwidth could be included in the "energy" function. When the "energy" is minimized, the relative sidelobe level is now also minimized. The beamwidth at the final run will be taken as the "specified" beamwidth with the final W_{mn} weights. The

relationship of beamwidth and sidelobe level is then optimum in the sense of Dolph-Chebyshev, that is, the sidelobe level is the lowest for the given beamwidth.

4.SIMULATION

Since the simulated annealing process is the same for a 2-dimensional array as for a 1-dimensional array and considering the limited computation power of the MICRO PDP-11 computer available in our simulation, a 1-dimensional array is used in our study. The 1-dimensional array is also assumed to be a continuous one with many desired pixels. Each of the pixels acts as a subaperture. The simulation starts with a uniform distribution (all subapertures with 1 or -1). The far field pattern is shown in Fig.2 (a) for this uniform distribution case. The distribution function is restricted to the set of 1, -1, which means real transmittance with binary phase (phase=0 or π) modulation. Then, simulated annealing is carried out by just changing the sign of each subaperture in turn, calculating the intensity of the highest sidelobe and applying the algorithm for each change. The final optimum result is given in Fig.2 (b). This simulation is done for an array of 41 subapertures. The subaperture size is assumed to be equal to the spacing A between subapertuers and is taken to be 61λ (figure relevant for optical arrays). The element distribution function that gives the final optimum result is shown in table 1. This function gives optimum pattern only for broad side direction (θ=0). Like the Dolph-Chebyshev optimum function, the optimum function given by simulated anneling is different for different steering angles, but an optimal weight can be computed for

each steering angle. From the simulation result, it is seen that the far field pattern has similar features to the pattern given by the Dolph-Chebyshev distribution function. In the Dolph-Chebyshev pattern, all the side lobes have the same level for a specified beamwidth. A numerical example in [1] shows an 8-element array (element separation $d=0.5\lambda$) with 25.8-dB sidelobe level and 40.8 beamwdth. The optimum pattern given by our simulation shows nearly equal level side lobes which are minimized for the given beamwidth.

5.DISCUSSION

Simulated annealing is a modification of the iterative improvement algorithm[4]. It is physically more meaningful and can be computed more systematically than the iterative improvement[4]. Physically, simulated annealing process is analogous to the cooling of atoms in crystal growth: careful annealing produces a defect-free crystal, rapid annealing produces a defective crystal or glass[3]. The probabilistic treatment with the probability function $P(\Delta E)=\exp(-\Delta E/KT)$ provides a way to accept the unfavorable changes and is much easier to compute. From our simulation, it has been found that the simulated annealing algorithm seems always to give better performance than the iterative improvement algorithm.

Since simulated annealing is a modified iterative improvement process, it takes a relatively long time to do an optimization problem just as iterative improvement does in a computer calculation. The phased array synthesis in our simulation runs for one hour or so for

an array of 41 elements on a MICRO PDP-11 computer. Finding an efficient scheme to reduce the excessive amounts of computer time on most optimum problems has always been of concern[5][8]. Otherwise, if enough computation power is available iterative improvement can be run from random starts for many times to approach the optimum state. Fast opto-digital computing schemes similar to those described in[9] may also be considered for phased array synthesis by simulated annealing. It is understood that the far field is the Fourier transform of the array distribution function. An optical lens can be used for computing the Fourier transform as the distribution function is inputed to the front focal plane of the lens via, for example, an appropriate compuer driven spatial light modulator (SLM). The Fourier transform in the back focal plane can be recorded and fed to the computer/controller to make the simualted annealing decision. The outcome is fedback to the SLM to change the distribution function in the front focal plane. This process can be repeated for every step in simulated annealing. The hybrid opto-digital scheme will do the Fourier transform instantly. In this fashion the computation time associated with the Fourier transform can be virtually eliminated assuming a high speed SLM and computer interface are utilized. An opto-electronic Boltzman machine for accelerating the selection rule has also been proposed earlier in [9]. Also, a Cauchy probability selection rule, instead of the Boltzman selection rule, can be used to speed up the whole annealing process further[8]. As claimed in [8], the computational saving of simulated annealing with Cauchy probability selection when comparied with the one with Boltzman selection is similar to that FFT comparied with DFT.

5. ACKNOWLEDGEMENT

This work was supported by DARPA/NRL and with partial support from the Air Force of Scientific Research and the Army Research Office.

REFERENCES

1. C. L. Dolph, "A current distribution for broadside arrays wich optimizes the relationship between beam width and side-lobe level", Proc. IRE. 34, pp.335-348, June 1946.

2. N. Metropolis, et al., "Equation of state calculations by fast computing machines", J. Chem. Phys. 21, pp.1087-1092, June 1953.

3. S. Kirkpatrick, et al., "Optimization by simulated annealing", Sience 220, pp.671-680, May 1983.

4. W.E. Smith, et al., "Reconstruction of objects from coded images by simulated annealing", Opt. Let. 8, pp.199-201, April 1983

5. B. Dunham, "Design by natural selection", Synthese 15, pp.254-258, 1963.

6. S. Lin, "Heuristic programming as an aid to network design", Network 5, pp.33-43, 1975

7. N. Farhat, "Radiation Pattern Analysis of an Infra-red Optical Phased Array", report submitted to RCA, Dept. of E. E., University of Pennsylvania, December 1985

8. H. Szu, "Fast Simulated Annealing with Cauchy Probability Density", Neural Networks for Computing Conference, Snowbird, Utah, April 1986

9. H. Barrett, et al., "Optical Boltzman Machines", Post-deadline paper, OSA Topical Meeting on Optical Computing, Incline Village, NEV.(1985)

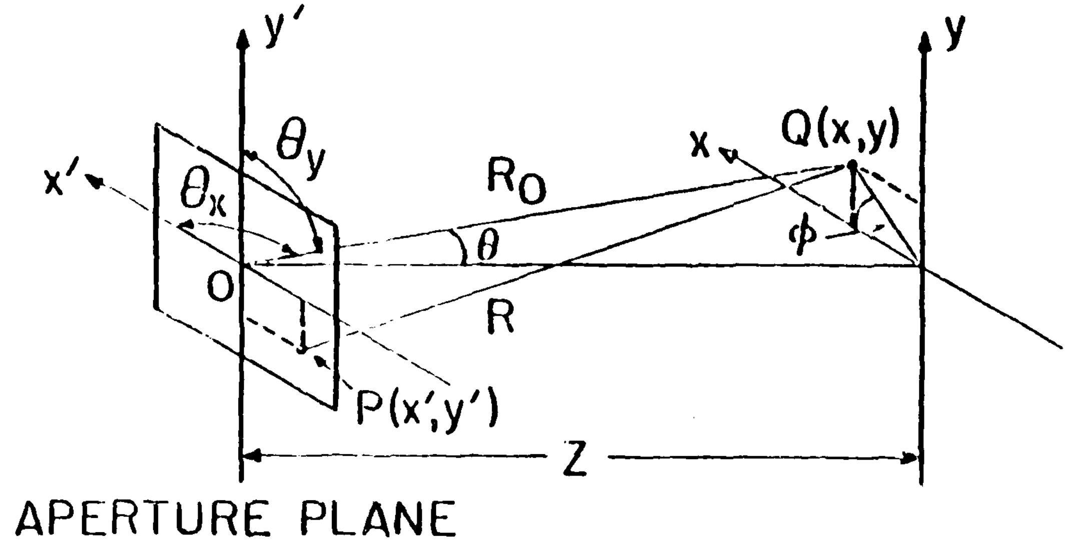

Fig. 1. Geometry for computing the far field radiation pattern of an aperture.

Simulated Annealing Synthesis

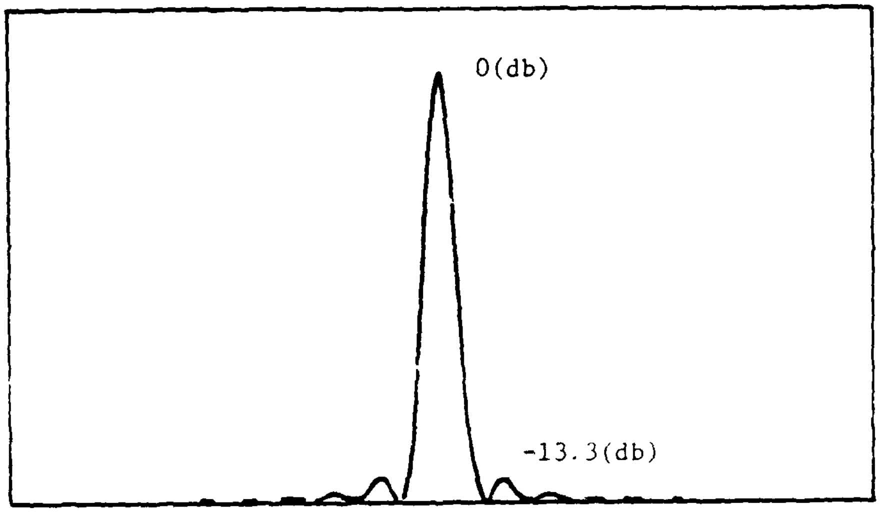

(a) mainbeam width: 4.58E-2(degree)
view range: [-0.004, 0.004]

Simulated Annealing Synthesis

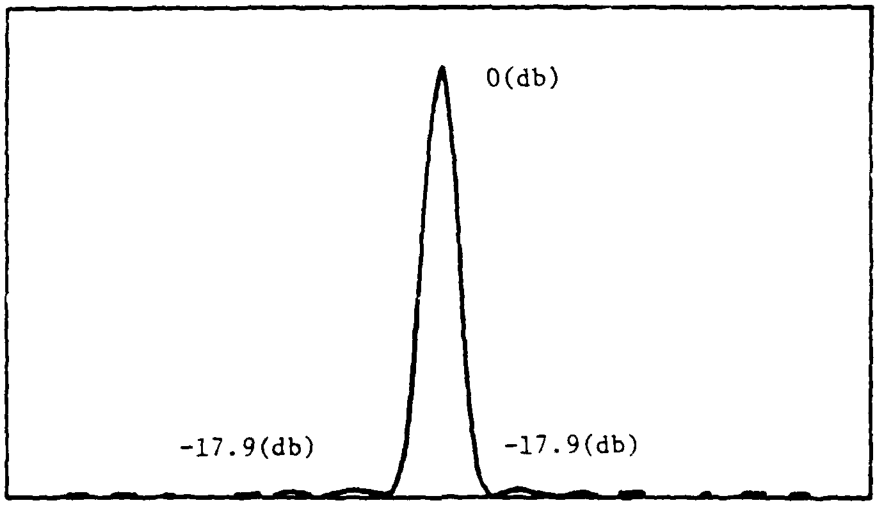

(b) mainbeam width:5.5E-2 (degree)
view range:[-0.004,0.004]
# of elements: 2*20+1=41

Fig. 2. simulated annealing result (a) for the uniform distribution
(b) the simulated annealing result

ELEMENT	-20	-19	-18	-17	-16	-15	-14	-13	-12	-11	-10	-9	-8	-7	-6	-5	-4	-3	-2	-1	0
WEIGHT	1	1	-1	1	1	-1	1	1	-1	1	1	1	1	1	1	1	1	1	1	1	1

ELEMENT	1	2	3	4	5	6	7	8	9	10	11	12	13	14	15	16	17	18	19	20
WEIGHT	1	1	1	1	1	1	1	1	1	1	1	1	1	1	1	1	1	1	1	1

Table 1. The Final Distribution Function Weights for the Optimum Pattern

END
DTIC
7-86